

POLITECNICO DI TORINO

Dipartimento Energia

Master of Science in Electrical Engineering

Academic Year 2019 - 2020

Master of Science Thesis

**Advanced Transient Thermal Modeling
of Traction Motors
in Ansys**



LUCA BOSCAGLIA
Prof. Aldo BOGLIETTI
Dr.-Ing. Shafigh NATEGH

March 2020

Whatever you do with your life, be a builder.

Tim Cock, June 2019.

To my family, always present in my life.

Abstracts

This thesis introduces the results of the study about the thermal modeling conducted through the collaboration between Politecnico di Torino and ABB AB.

The Aim of the project is to become a reference for the definition of an innovative thermal model relative to an asynchronous motor for railway traction.

Calculations are done in Ansys and are then compared with the results obtained in the ABB laboratories.

The thesis can be divided in four main topics.

The first chapter is concentrated on different cooling layouts for electric motor, operating conditions of traction motors and different thermal modelling methods.

The second chapter deals with all the challenges that a thermal analysis and the design of a thermal model can bring about motors in the railway field. All the CFD calculations are made with ANSYS. Finite elements analysis is introduced paying attention to Finite Volume modeling also since it will be used by the simulator as well. The 3D design of the motor and fan are made with ANSYS SpaceClaim and a CFD simulation is conducted with ANSYS Fluent.

In the third chapter thermal models developing for railway traction motors are described

At the end, in the fourth chapter, the results obtained are compared with the experimental ones in the laboratory.

Contents

Chapter 1: Introduction	6
Chapter 1.1: Traction motors cooling layouts	8
Chapter 1.2: Traction motors operating conditions	12
Chapter 1.3: Different thermal modeling methods	13
Chapter 1.4: Analytical Approach	13
Chapter 1.5: Numerical Methods	15
Chapter 2: Numerical modeling of the cooling flow	16
Chapter 2.1: Introduction: Fan basic and selection criteria	16
Chapter 2.2: Finite element vs. finite volume	22
Chapter 2.3: 3D modeling of the fan.	25
Chapter 2.4: Boundary conditions	28
Chapter 2.5: Solver setup	30
Chapter 2.6: Mesh setup	31
Chapter 2.7 Fluid velocity results	32
Chapter 3: Computational Fluid Dynamics (CFD) of Traction Motor	37
Chapter 3.1: Introduction: modeling challenges for Railway Motors.	37
Chapter 3.2: 3D Modeling of the motor cooling system	38
Chapter 3.3: Boundary conditions and solver setup.	41
Chapter 3.5: Mesh setup.	42
Chapter 3.6: CFD results.	43
Chapter 4: Conjugate Heat Transfer Model (CHT)	46
Chapter 4.1: Most difficult aspects of electrical machines thermal modeling.	46
Chapter 4.2: Winding and end winding model.	47
4.2.1 Finite Element Method.	47
4.2.2 Analytical Approach based on Homogenization.	49
4.2.3 Experimental Approach: Short Transient Test.	51
Chapter 4.3: Thermal resistances implementation	58
Chapter 4.4: Heat sources and material settings.	60
Chapter 4.5: Steady-state thermal results.	62
Chapter 5: Reduced-Order thermal Model (ROM)	68
Chapter 5.1: Introduction: transient simulation based on Machine Learning.	68
Chapter 5.2: ROM transient results.	71
Chapter 6: Experimental Setup: model validation.	72
Chapter 6.1: Case Study Motor.	72
Chapter 6.1: Airflow measurements.	73
Chapter 6.2: Temperature measurements.	76
Chapter 7: Conclusions and future work.	79
Publications	81
Chapter 8: Bibliography	82
Acknowledgments	

Chapter 1: Introduction.

Thanks to the large numbers of benefits, electric motors are increasingly used in the automotive and railway traction fields. They are able to work with a significant reduction of emissions and can be controlled with high performances according to different demands.

At the beginning of the 20th century, in the railway traction, DC motors for their high starting torque and ease of control were dominants. Subsequently, due to numerous mechanical components like commutator lamellas and the brushes that required continuous maintenance, the market has increasingly directed on the use of AC motors. Consequently, the attention in this thesis is focused on the AC traction motors.

Induction motors have the advantages of a low price, robustness and the possibility of being connected in series with the aim of increasing the power produced by using a single power converter, with a clear advantage from an economic point of view.

The high power and torque density combined with the need to use the motor at its maximum capacity require to study a suitable cooling like a forced-ventilation where the thermal stress is reduced, but more space for the air ducts and the external fan is requested. For these reasons to maximize the performance as well as the economic profits, it is necessary not only an optimal electromechanical design, but also to combine it with an efficient thermal modeling studied at design phase.

As well as the use of compact drives, even an optimal thermal model can lead to space savings where required, such as in applications like metros where the reduction of space is essential for the creation

of new seats. In this case a self-ventilated motor with a shaft mounted fan should be considered more convenient because the space for the air ducts is not needed.

Running the electric machines at their thermal capacity makes necessary to dimension them in transient conditions with their working duty cycle instead of steady state based on just one operating point. In this way a more complex thermal model can be obtained to enable transient thermal calculations for duty cycle in the ranges of hours.

To define the thermal model a Lumped Parameter method (LP) is used. It consists in representing distributed fields as scalar values in order to get quick results with a good precision assuming that the thermal parameters are estimated with high accuracy.

Many advantages can be obtained through a combination of a numerical and analytical approach. The model designed is constructed from a FE-LP model to design the geometric part, define the properties of the materials and impose the losses as input to the system. Successively the CFD results obtained at just one operating point to calculate the convective heat transfers are applied as boundaries conditions to the FE-LP model to get the solution. This combined approach gives a lot of benefits like the reduction of computation time and a better modeling of complex parts (stator and rotor lamination, stator coil, rotor bars...etc) modeled in FE and of the end-parts modeled analytically.

The possibility of having a good thermal modeling is in line with today's needs. In recent years, the tendency to lower the life-cycle costs of components in railway applications is leading to longer maintenance intervals. Having long intervals of maintenance causes an inevitable accumulation of dirt which is a problem especially if this happens in the rotor and stator ducts preventing a proper cooling. This affects especially the bearing and the winding insulation systems whose lifetime is very temperature sensitive.

Consequently, any thermal model, at most developed for this kind of application, should be able to model this kind of phenomena e.g. dirt accumulation

1.1 Traction Motors Cooling Layout

In the railway traction, higher motor performance is required with very high torque and power densities. A high-power density can be achieved through high current densities, but these currents increase the copper losses and, in turn, the temperature. Another method of increasing power density is running at a higher rotation speed. This would increase the frequency with consequent iron losses in the stator and rotor steel laminations and an increase in rotor temperature would be unfavorable as it is very difficult to cool down.

Numerous efforts have been made to improve the cooling system of electric machines. First by improving the heat transfer in particular hot spots like housing fins, rotor surfaces and end windings through forced air. As current densities increased, this was no longer enough, and cooling was achieved with cooling liquids like water or oil. The water may be used in machines that are not difficult to cool like motors with short end windings. Directly oil cooled motors, otherwise, can be employed in applications with larger number of poles where the end windings are longer.

Another distinction can be made between forced-ventilation cooling and self-ventilated motors. The first have the advantage of providing the motor with a constant and clean cooling that makes it less sensitive to environmental conditions and to the operating point. In the other hand this kind of cooling takes away a lot of space for the external fan and rotor ducts, so it is realized where the space is not a problem like locomotives, and not where the size can reduce the number of seats such as the metros. Open self-ventilated motors have shaft mounted fans with no air ducts and external propellers, although for dirty environmental operating conditions a closed self-ventilation may be preferred.

Considering the motors running in duty cycle, the goal of the thermal designing is to predict the loss variation in the several parts of motors and limit the temperatures in the critical parts including windings and bearings. The thermal project and choice of the cooling type depend on the accuracy of this prediction and the duty decided.

Several methods of cooling of induction motors for railway use are now illustrated.

A) Open Air Forced-Ventilated Cooling

This kind of cooling is used for locomotives and Electric Multiples Units (EMUs) in both framed or frameless designs.

Forced-Ventilates Cooling means that the cooling is supplied by an external fan through the air ducts.

The cooling is influenced solely by the internal pressure drop across the motor and its operating conditions are not limited by the speed and the operating point of the machine. In this way a forced-ventilates cooling can reach high torque and power densities which are not allowed to the self-ventilated one where they are directly linked to the motor's speed increasing the losses.

The forced-ventilated motors have got several benefits:

- the aeroacoustics noise is not an issue;
- cooling operating conditions independent by operating point of machine.
- good air quality due to the low amount of pollutants that reduces the possibility of blockages in the air ducts

Disadvantages:

- an external fan is needed;
- space for air ducts is requested.



Fig.1.1 - Frameless forced ventilated



Fig. 1.2 - Framed forced ventilated

B) Open Air Self-Ventilated Cooling

This is the most used for metros and it is realized by using a radial shaft-mounted fan. The cooling of the inner surfaces is realized by an open-circuit flow of the ambient air.

The main characteristic of self-ventilated cooling is the heavy dependency of the cooling to the machine's operating point. The volume flow rate depends on both the pressure drops across the motor and the fan design, as well as the motor speed.

The open air self-ventilated cooling presents several advantages:

- simple design;
- external fan not needed;
- space for air ducts not requested.

Disadvantages:

- the cooling is strongly dependent to the motor's speed, so it decreases at lower speeds (<1000 rpm);
- higher noise levels at high speeds (>4000 rpm).

The gear ratio for this kind of motors is limited. This means not only that the motor size and weight are reduced but also that the cooling capability decreases because of the average speed reduction. That is done to limit the mechanical stress of rotating parts and the noise level, but the outer fan diameter cannot be reduced under certain limits to guarantee an elevated air flow in order to front a big amount of dirt, and avoid particle accumulation in the ducts.



**Fig. 1.3 - Open air self-ventilated
electric traction motor**

C) Enclosed Air Self-Ventilated Cooling

The air self-ventilated cooling can be divided in two regions: an internal regions and external regions. In the external regions there are one or two radial shaft-mounted fans that provide air flow

through ducts in the stator laminations. In the internal regions the cooling is provided by wafters mounted on the rotor short-circuit ring that pump air around the stator end-windings.

This method is often used for bad environmental conditions characterized by a large amount of dirt particles in the air (e.g. inner-city trams) and with Permanent Magnet motors where a clear separation between magnetic and metallic parts is needed.



**Fig. 1.4 - Enclosed air self-ventilated motor
electric traction motor**

D) Enclosed liquid Cooling

A lot of cooling systems now include coolants. Such liquids like water and oil circulate in controlled paths in order to promote the heat transfer through the cooling ducts in the housing.

Since the water cannot touch the stator and rotor steel laminations, the motor is provided with an housing water jacket.

Using liquid cooling like water can bring several advantages like the reduction of aero-acoustic noise and mechanical vibrations. In comparison with air ventilated cooling we can surely consider the enclosed liquid cooling with a more compact design as well. In the other hand the main disadvantages of this kind of cooling can be considered the difficulty to cool the end windings e.g. in the case of few numbers poles motor with larger end windings. To improve the cooling different solution can be implemented like potting.

1.2. Traction motors operating conditions

The thermal behavior of traction motors is studied when they run in a duty cycle and losses are distributed along the whole period considered. This make necessary to apply our studies about thermal modeling during the design-phase in transient based on working duty cycle instead to observe the thermal performance in steady state condition corresponding to a specific operating point.

The aim of the thermal model becomes in this way to predict the temperature variation in the critical parts of motors in order to limit the thermal stress in particular hot spots of windings and bearings. The thermal designing and the cooling method used depend on the accuracy of this prediction that can be done in a duty cycle.

An example can be showed, in figures 5 and 6, with a typical duty cycle and presents how stator winding and bearing temperatures changes as a function of time by varying motor torque and speed. In this case there is a comparison between the temperature measured and estimated using the thermal model.

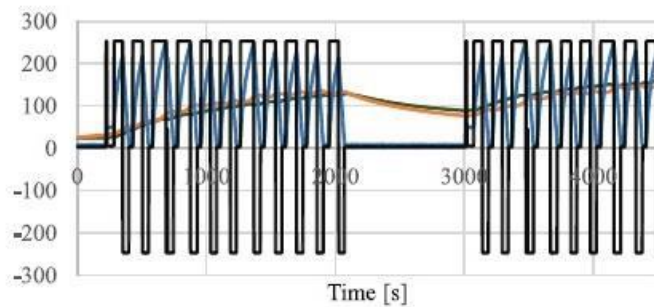


Fig.1.5 - Comparison between estimated (brown) and measured (green) temperature of the end winding, with specific torque (black) and speed (blue)

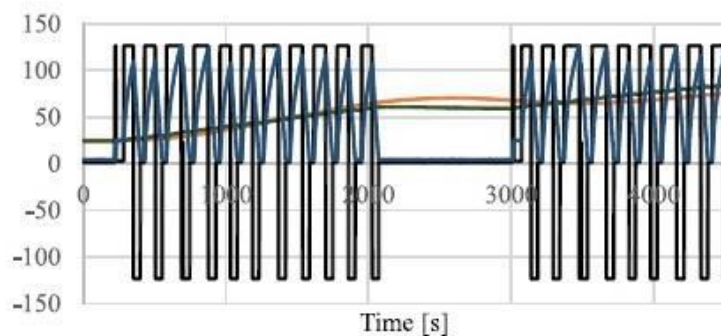


Fig.1.6 - Comparison between estimated (brown) and measured (green) temperature of the bearing, with specific torque (black) and speed (blue)

In both these figures, torque increases positive and negative and then it becomes constant. The speed (blue line) has got a ripple but then stays to zero because in this interval of time the train is stationary. Consequently, the temperature of the winding (in brown estimated and green measured) increases up to 2000 s, then decreases until 3000 s and then increases again. The thermal behavior of bearing is very close to the windings one. The only differences are about the higher thermal capacity and the temperature (in brown estimated and green measured) that is less load and speed sensitive.

1.3. Different thermal modeling methods

The thermal model employed is implemented as a combination of analytical and numerical methods:

- Lumped Parameter thermal modeling (LP);
- Computational Fluid Dynamics modeling (CFD);
- Finite Element modeling (FE).

The first one is analytical, the second and third are numerical.

They can be used independently of each other in combination to obtain particular improvements such as shorter calculation times or better estimation of results.

1.4 Analytical Approach.

The Lumped Parameter approach is the most using in the thermal modeling.

A LP model is a represent like an electrical circuit , where spatially distributed fields are replaced by single scalars values. In the fig. 8 an example about an electrical machine is showed when every parameter is represented like a block and it is defined according to the material and component properties. In these schemes the conduction is represented by dark blue blocks, convection and radiation are represented by light blue blocks.

Inside a LP model the losses are the inputs and they are modeled like heat sources.

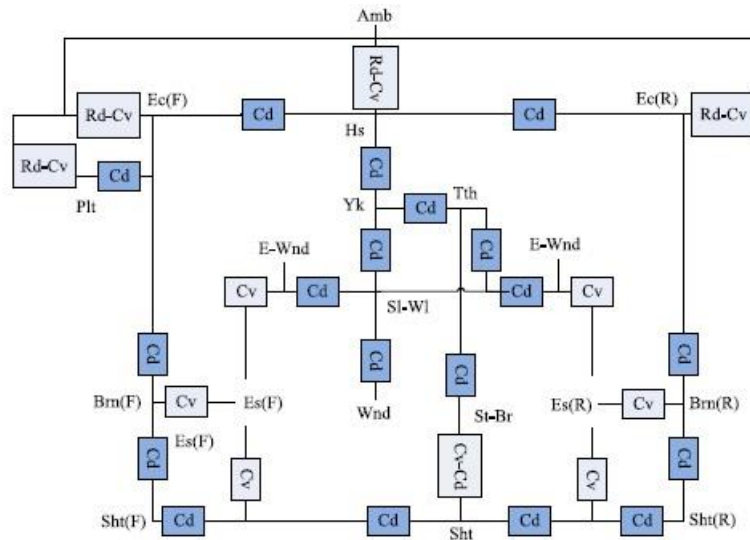


FIG. 1.7 - Example of lumped parameter thermal model of electric motor.

TABLE I.I
ABBREVIATIONS SYMBOLS

Symbol	Abbreviation	Symbol	Abbreviation
F	Forward	Hs	Housing
R	Rear	Plt	Plate
Cd	Conduction	Sht	Shaft
Cv	Convection	Sl-Wl	Slot wall
Rd	Radiation	St-Br	Stator bore
Brn	Bearing	Yk	Stator yoke
Ec	End cap	Tth	Stator tooth
Es	End space	Wnd	Winding

Thermal model obtained only with analytical approaches cannot be used to model accurately the thermal effects of complex structures of electric motors. Even though this modeling method is pretty simple and fast it may not be easy used to model thermal effects of complicated parts like the windings.

For these reasons also numerical approaches are needed.

1.5 Numerical Methods.

Finite element analysis (FEA) and computational fluid dynamics (CFD) are the numerical methods used for thermal analysis of electric machines. In FE model, conduction in solid elements with their conductivities can be modeled accurately. The FE method models the stator coils, stator lamination, housing, rotor bars and rotor lamination.

3D CFD calculations has the aim to model the distribution of the air between the stator ducts, air gap and rotor ducts. Also, the CFD calculation results provide an estimation of the air velocity in the motor end parts. The used software for CFD calculation is ANSYS FLUENT.

Another use of the CFD calculation in the method suggested is to calculate the fan operating point. It is very important to highlight that rotor rotation and its influence on pressure drop in the motor are included in the model proposed.

The author would like to thank eng. Fabio Bonsanto and the Ansys team for their efforts and contribution in this chapter.

Chapter 2: Numerical modeling of cooling flow.

In this chapter a numerical model of cooling flow is presented. At the beginning the physic of the fan is briefly treated. The proposed modeling approach using Ansys tools for the CFD simulation is evaluated on a basic model formed by the fan and the air guide only.

Chapter 2.1: Introduction: fan basics and selection criteria.

A fan is a powered machine that converts electric and mechanical energy into aerodynamic energy.

This energy is represented by two main parameters:

Static pressure (SP): it is defined as the pressure exerted by the fluid on the walls of the pipe or vessel in which it is contained. It acts equally in all directions and is independent of the velocity of the fluid. Taking the ambient pressure as a reference, the static pressure is positive when it is greater than the ambient pressure, negative when it is less.

Kinetic Energy: the fan not only increases the pressure behind it but also accelerates the particles of air. In their movement they loose kinetic energy because of the collisions with each others and

walls, and in form of turbulence and vortices. Expression of the kinetic energy is usually the cubic feet per minute (CFM) called volumetric flow rate which, by the way, does not change with altitude.

The total pressure, indeed, is given by the sum of two addends, from the conservation of fluid momentum :

$$p_s + \rho \frac{u^2}{2} = \text{constant} = p_t$$

p_s is the Static Pressure

$\rho \frac{u^2}{2}$ is the Velocity or Dynamic Pressure

p_t is the Total Pressure.

The conservation of momentum states that *within some problem domain, the amount of momentum remains constant; momentum is neither created nor destroyed, but only changed through the action of forces as described by Newton's laws of motion.*

Let us consider a fluid like the air entering into a domain with inlet section 1 and outlet 2. For example the simplest case is considered with just one dimension and steady state condition like in the Fig. 2.1

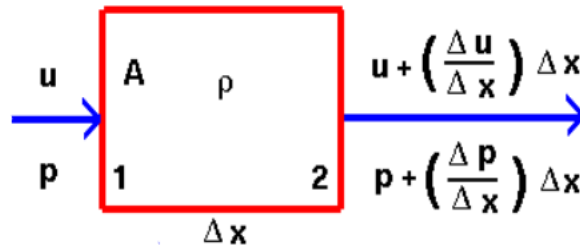


Fig. 2.1

x = distance	A = area
u = velocity	F = force
a = acceleration	P = pressure
t = time	ρ = density
m = mass	

The velocity at 2 is given by the velocity at 1 plus gradient times the distance. The same for the pressure.

$$u_2 = u_1 + \frac{\Delta u}{\Delta x} \Delta x$$

$$p_2 = p_1 + \frac{\Delta p}{\Delta x} \Delta x$$

Considering the Newton's Second law:

$$F = ma = m \frac{\Delta u}{\Delta t}$$

$$F = -[(pA)_2 - (pA)_1] = m \frac{u_2 - u_1}{\Delta t}$$

The area A and the density ρ are constant. Since the pressure increases with the x (from a region with higher pressure towards a region with lower pressure) and the velocity decreases with the x, there is a minus at beginning.

$$-\left[\left(p + \frac{\Delta p}{\Delta x} \Delta x\right) A - pA\right] = m \frac{u + \frac{\Delta u}{\Delta x} \Delta x - u}{\Delta t}$$

$$-\left(\frac{\Delta p}{\Delta x}\right) \Delta x A = m \frac{\Delta u}{\Delta x} \frac{\Delta x}{\Delta t}$$

where $\frac{\Delta x}{\Delta t} = u$

$$-\frac{\Delta p}{\Delta x} = \rho u \frac{\Delta u}{\Delta x}$$

Differential form

$$-\frac{dp}{dx} = \rho u \frac{du}{dx}$$

This is a one-dimensional, steady form of Euler's Equation.

Integrating the last equation, we get a form of the Bernoulli's Equation that gives us back the Dynamic Pressure expression above:

$$p_s + \rho \frac{u^2}{2} = \text{constant} = p_t$$

The two parameters, static pressure and flow rate, are used to measure the fan energy output and in particular to realize how much static pressure alone can the fan bring to bear upon the air (shut-off condition), and how much kinetic energy alone can the air through the fan involve (free-delivery condition).

They are used to build the most important characteristic of a fan named "fan curve".

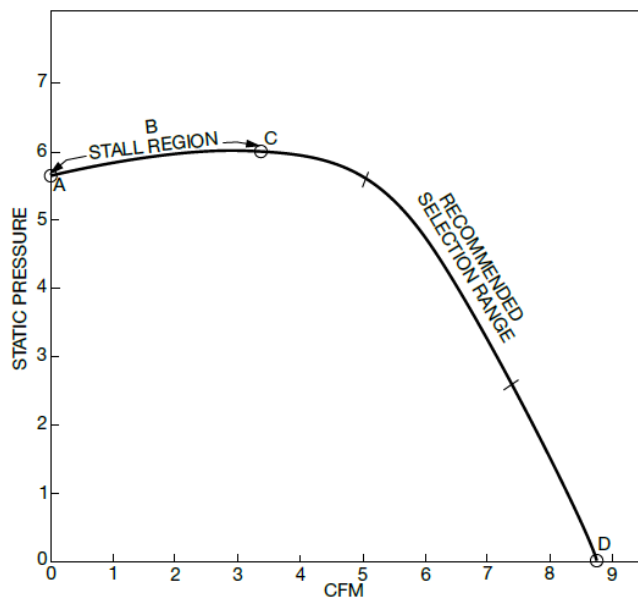


Fig 2.2 Classic Fan Curve

A fan curve is a pressure-CFM characteristic as the one illustrated in Fig. 2.2 where a centrifugal fan has been considered as example.

Point A is usually named "shut off" and it depicts the fan curve's point where there is no airflow. Being the volumetric flow equal to zero the velocity pressure will be naught. In this condition there is the maximum static pressure, then the maximum potential energy.

Point B represents the “stall region” : it is not recommended to work there since it is characterized by an erratic value of flow rate that produces immoderate vibrations and noise.

Point D is known as “free delivery” point. This case has the maximum kinetic energy and zero static pressure.

The CFM-SP curve depends also by the kind of fan.

The fan types are mainly classified based on how the air passes through the impeller.

In the axial flow fan the air runs in an axial direction creating a swirling tangential motion caused by the blades (Fig. 2.3)

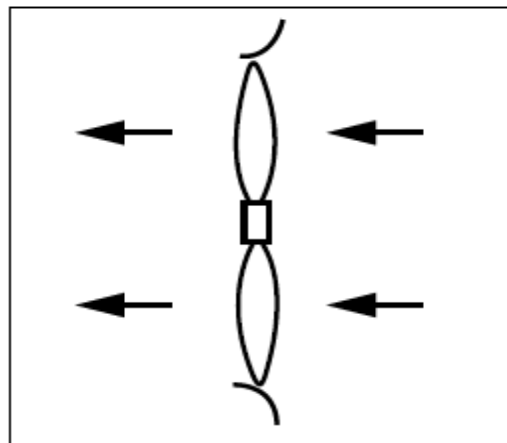


Fig. 2.3 Tangential motion created by axial flow fan

By the rotation and the relative tangential forces generated, the axial fan increases the air velocity. In this way an high value of dynamic pressure and kinetic energy is reached with a small static pressure and potential energy production.

In the centrifugal fan the air flows through the impeller axially and then its acceleration is increased by the blades that discharge it radially. In this case a rotating air volume is produced generating both potential and kinetic energy.

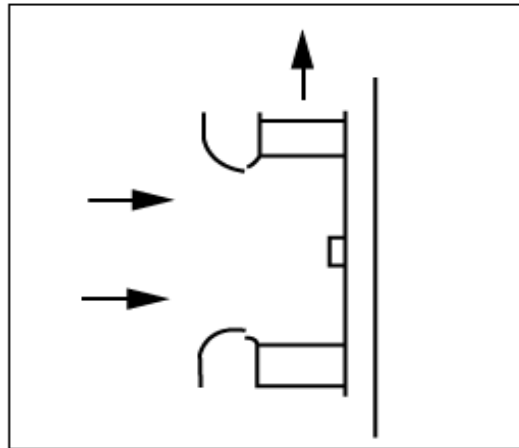
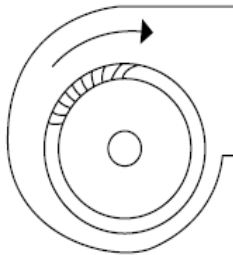


Fig. 2.4

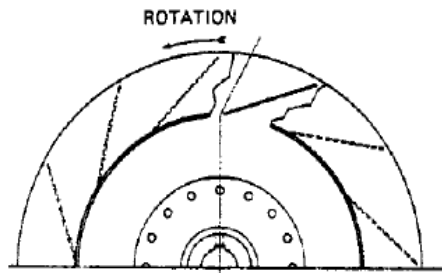
According to different blades designs, the centrifugal fans can be classified into several types:

- Forward curve
- Backward inclined
- Radial or straight blade.

Forward Curve Fan



Backward Inclined Fans



Radial Blade

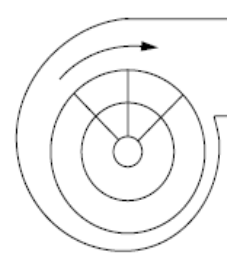


Fig. 2.5

For each type we can consider the respective speed triangle as shown in Fig. 2.5

The resultant velocity vector is the longest for the Forward Curve fan, the smallest for the Backward Curve ones, otherwise there is something in the middle for the Radial Curve impellers.

Different blades shapes have advantages and disadvantages, depending of the applications, the wanted flow speed and the direction of the coolant requested.

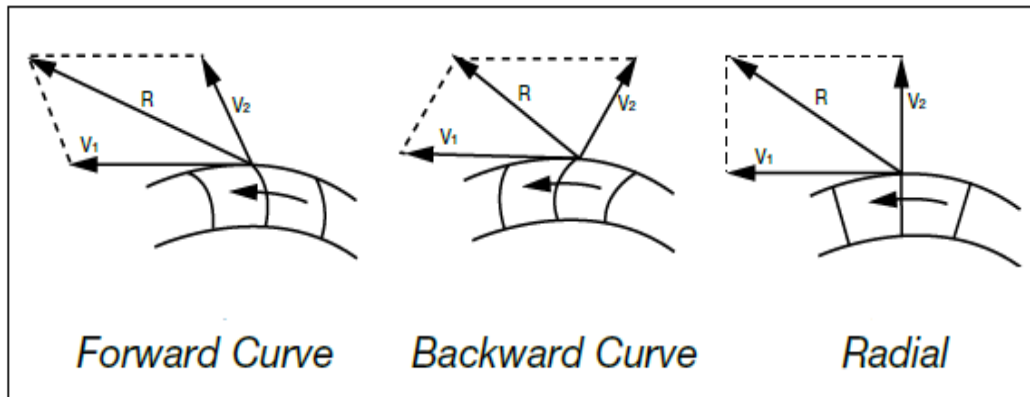


Fig. 2.6 Velocity triangle for different centrifugal fans

One of the most used are the Forward. These fans have the highest operating speed of all centrifugal fans, and they loss less energy to convert the dynamic pressure into static pressure along the housing than all the others. All this is paid with higher price and a very detailed construction of the blades.

The Forward Curve fan has the advantages of a relatively high airflow with a low speed and quiet operation. This makes it very suitable for residential and commercial cooling and heating. The high horsepower requirement close to the free delivery point and its lack of robustness make this type of propeller not very used in the industrial field.

The Radial Curve Fans are commonly used for their constructive simplicity and their rugged construction. They are mostly used in the industrial market due to their high noise level and the ability to manage air flows with high levels of particulates.

Chapter 2.2: Finite element vs. finite volume.

In a CFD method the resolution of a partial differential system can be solved by decomposing the system into several algebraic equations.

The three most used CFD calculation methods are:

- Finite Difference
- Finite Volume
- Finite Element.

In the first method, the partial derivatives are replaced with Taylor series truncated to the first or second term. Obviously more terms of the series are introduced more the method of calculation

would become precise, but at the same time the computation would become too onerous due to the too high number of nodes and discrete points.

In the case of simple geometries this method is rather simple to apply. Instead, in the case of complex and irregular geometries it requires a transformation of the equations before applying the Taylor's series, which can lead to meshing and convergence problems.

In the second method, considering a linear variation of the separate independent variables that govern the differential equations, an integration is performed on a finite volume element. Considering single elements of volume, the resolution is reduced to the verification of the mass and energy balance in the volumetric domain. Since it is necessary to calculate the flow between all the neighboring nodes, in the case of non-regular meshes such as the tetrahedral ones, the number of flows to be calculated would become very large, and consequently the effort to ensure the correct calculations is very high.

In the third method, the Galerkin's method of weighted residuals is used. It is based on differential partial equations that are first multiplied by a weight function and then integrated onto an element or volume. The main difference compared to the previous method is that Finite Elements doesn't work on flow functions but on shape function. On the one hand this is a disadvantage because it is difficult to attribute any physical meaning to these terms, on the other it represents an advantage since the calculation with the Finite Elements does not depend on the type of geometric shape considered.

Method	Advantages	Disadvantages
Finite Element	<ol style="list-style-type: none"> 1. More mathematics involved 2. Natural boundary conditions (for fluxes) 3. Master element formulation 4. Any shaped geometry can be modeled with the same effort 	<ol style="list-style-type: none"> 1. More mathematics involved - less physical significance
Finite Volume and Finite Difference	<ol style="list-style-type: none"> 1. Fluxes have more physical significance 	<ol style="list-style-type: none"> 1. Irregular geometries require far more effort

Figure 2.7 Advantages and disadvantages of Finite Element and Finite Volume Methods

The upsides and downsides for the utilization of finite element or volume are listed in Fig 2.7.

This thesis is focused on CFD analysis made with Ansys tools.

Ansys Fluent solver is based on the finite volume method:

- the domain is discretized into several control volumes using a computational grid.

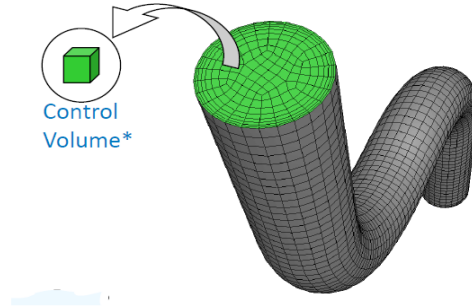


Fig. 2.8 Exemplification of Finite Volume Method

- considering this set of volumes, general transport equations are integrated on each control volume:
 1. continuity equations (conservation of mass);
 2. momentum equation (Newton's second law);
 3. energy equation (conservation of energy).
- Partial differential equations are discretized obtaining a system of algebraic equations. These are then solved to represent the solution field

<u>Equation</u>	<u>ϕ</u>
Continuity	1
X momentum	u
Y momentum	v
Z momentum	w
Energy	h

Fig. 2.9 Equation Calculated for each finite volume

$$\underbrace{\frac{\partial}{\partial t} \int_V \rho \phi dV}_{\text{Unsteady}} + \underbrace{\oint_A \rho \phi \mathbf{V} \cdot d\mathbf{A}}_{\text{Convection}} = \underbrace{\oint_A \Gamma_\phi \nabla \phi \cdot d\mathbf{A}}_{\text{Diffusion}} + \underbrace{\int_V S_\phi dV}_{\text{Generation}}$$

Fig. 2.10 Differential equations solved by the method.

The thermo-fluid dynamics simulation that will be described in this chapter follows the items of a standard CFD simulation. It can be resumed as in Fig. 2.11

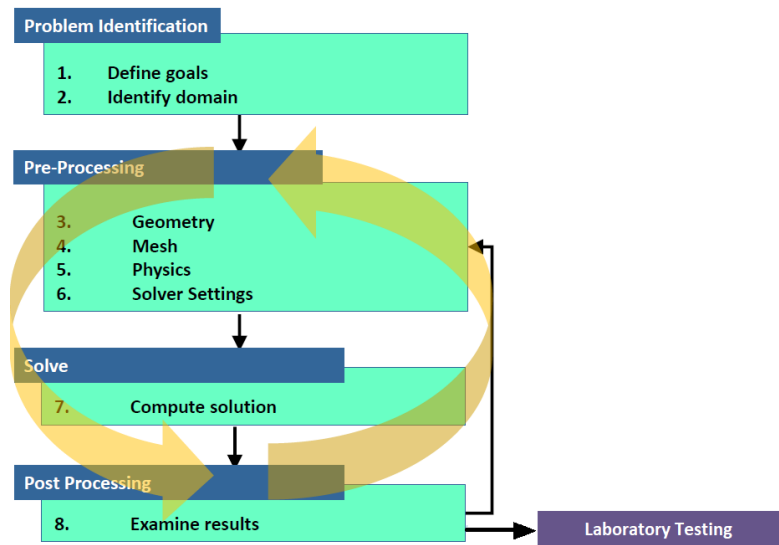


Fig. 2.11 Summary of the method used in this study.

The goal of this analysis is to get the static pressure- flow rate curve and the render of the velocity field.

The final results, then , will be compared with empirical ones obtained in the ABB laboratories.

Chapter 2.3: 3D Modeling of the fan.

After defined the goals, the first step consists in defining the fluid domain, in this case the air, for the thermo-fluid dynamic analysis.

The considered fan is a radial type designed by ABB's mechanical engineers. An air guide is also considered to direct and accelerate the airflow. The fan and the air guide are shown in Fig. 2.12 and Fig 2.13 respectively.

In this study only the cooling system is considered, and the motor is not included in the model yet.

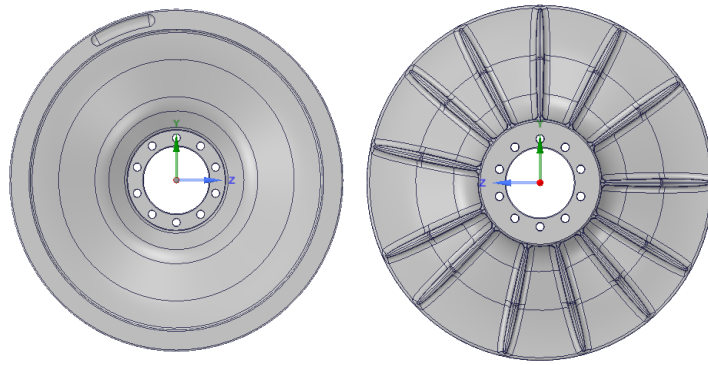


Fig. 2.12 Radial Fan of the case-study motor designed by ABB.

As shown in fig. 2.14 the model presented is formed by the propeller and the air guide, and the housing, as it will be possible to see later, is going to be replaced by an ideal enclosure at this level of the study.



Fig. 2.13 Air guide

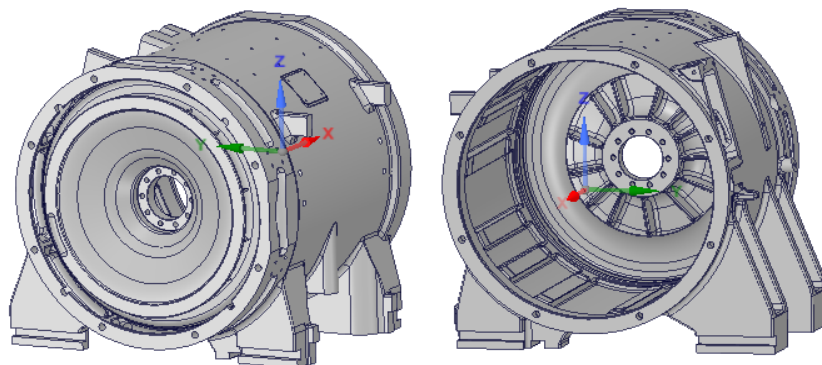


Fig. 2.14 Cooling System and housing.

To make the model operative for a CFD analysis a fluid domain has to be defined. For this purpose it is imported in Ansys SpaceClaim and the volumes are extracted.

More precisely the set formed by fan and air guide is inserted in a volume called rotating volume and in turn this one is inserted in an static enclosure named static volume. Then, there is a further cylindrical volume in substitution of the housing where the motor would be contained. It is important to stress that the volume of the solid parts has been extracted and only their respective surfaces considered. More specifically, only the “negative volumes” are in the model and the solid present neglected. This is done in order to take into account the fluid and the surfaces wet but the fluid itself.

The result is a fluid domain with no solid part ready for the CFD calculation as shown in fig. 2.15.

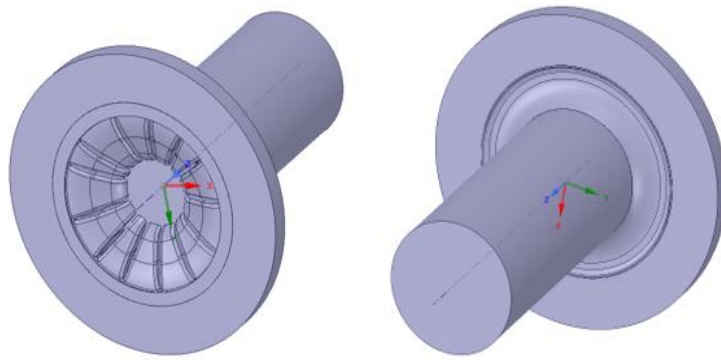


Fig. 2.15 Fluid domain of the fan model

It is necessary to remember that to carry out this operation it is always a good idea to simplify as much as possible the geometries involved removing, when possible, unnecessary features that would complicate meshing.

Chapter 2.4: Boundary conditions.

Defining the boundaries conditions is essential to assign the direction of the airflow and therefore to identify the boundaries of the model studied. For this reason, inlet and outlet are defined through a

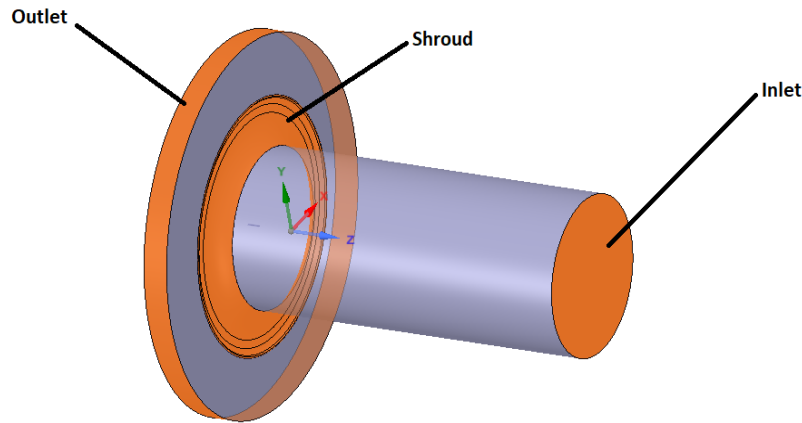


Fig 2.16 Boundary conditions

"group" creation in SpaceClaim. As shown in Fig 2.16 there is also another group selection named "Shroud". This is done to take into account the wall effect provided by the air guide since it helps to direct the airflow by increasing the pressure end speeding up the velocity.

In this case since the aim of this model is to obtain the curve of the fan, the boundary conditions to set are *pressure inlet* equal to zero and *mass flow outlet* set for different value of mass flow rate to have a reasonable range to calculate the curve. In this way, calculating the pressure at the outlet for each value of mass flow inlet, the pressure obtained will be the Static Pressure and the fan curve is defined.

Furthermore, the definition of boundaries condition is very important at the level of meshing. Since there are steep gradients of flow variables near the wall due to the boundary layers as shown

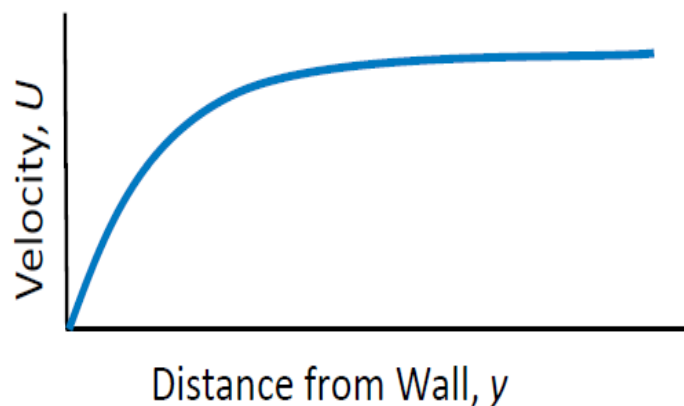


Fig. 2.17

in fig 2.7 , they bring necessity to fine mesh to resolve it. So, walls need inflation layers and this inflation has not to be applied to the outlet and inlet where the gradient is close to zero.

First of all, we need to identify the volume zones in movement of the domain and the stationary ones. The only part put in rotation must be the rotating volume: for the aforementioned part will be used the *frame motion* function at a defined angular speed.

The MRF model (The Multiple Reference Frame Model) is an easy way to approach multiple zones problems. It can be considered a steady-state approximation where individual cell zones are moving at different rotational speeds, and it is possible to use it when interfaces are surfaces of revolution about rotational axis. In practice the fluid domain is divided in more zones where there are both moving and stationary volumes. The airflow in the moving cell zone is calculated using the moving reference frame equations. On the contrary in the stationary ones ($\omega=0$), the stationary equations are used. At the interfaces between each other's, appropriate transformations of the velocity vectors and gradients are applied, and locally fluxes of mass, energy and momentum are estimated.

It is important to highlight that the MRF approach does not take into account the relative motion of a moving zone with respect to the others (which can be stationary or not); the grid and meshes remain fixed with the time. This is equal to freezing the rotation of the moving parts in a specific position and consider the instantaneous flow field with the rotor in that precise position. For this

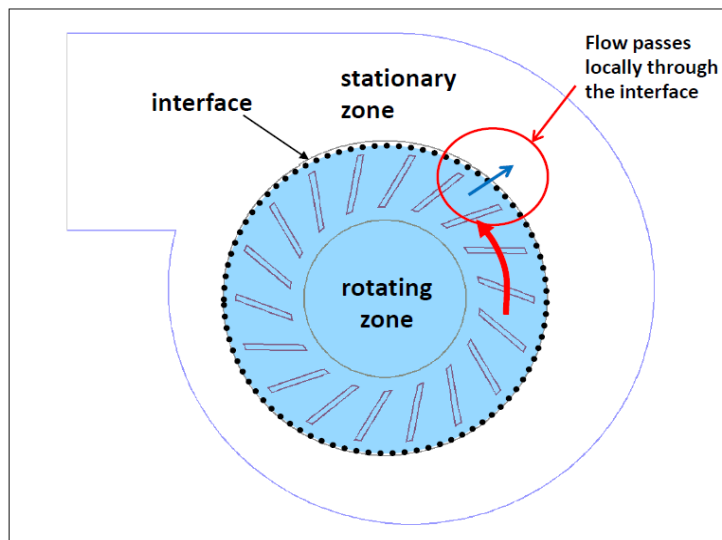


Fig. 2.18 Frozen Rotor Illustration

reason MRF is also called the "frozen rotor approach."

At last, in order to get the fan curve, as abovementioned particular initial conditions are applied:

- The inlet is set as *pressure inlet* in order to fix the pressure value at zero and estimate the pressure drop along the domain.
- The outlet is set as *mass-flow outlet* with the purpose of configuring the flow rate values like input parameters for the design points of the curve.

Chapter 2.5: Solver setup.

For a good CFD simulation the kind of turbulence must be identified.

The Reynold's number gives an idea about it and it determines the kind of turbulence as shown in Fig.2.19.

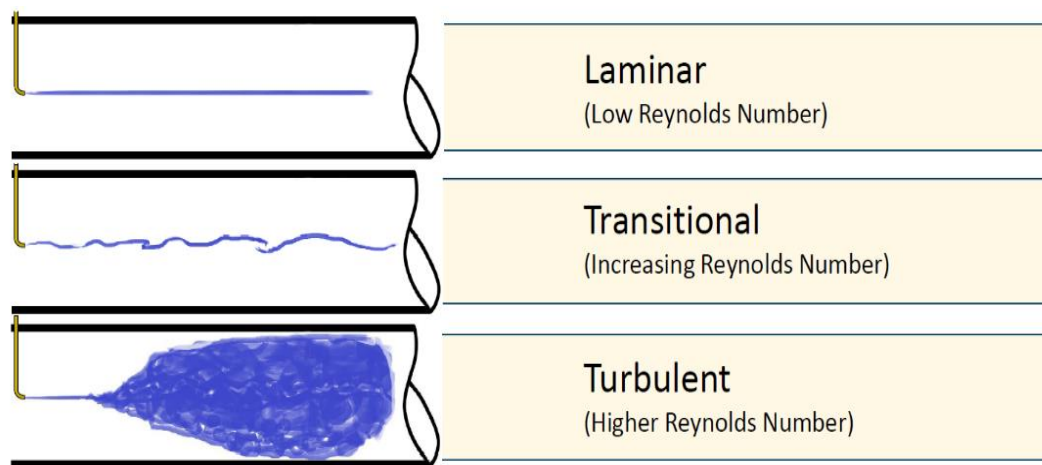


Fig. 2.19 Type of the turbulence models based on Reynolds Number variation.

Fluent offers different turbulence models each of them can fit different scenarios. The most common ones used for a wide range of CFD problems are the *Two-equation Models* as shown in Fig.2.20. They are characterized by a more accurate solutions but at the same time increase the computation time heavily compared to the *One-Equation Model*. This is the reason why going towards *Reynolds Stress* and *Transitions Models* the computational cost for each iteration is so high that they are very rarely used.

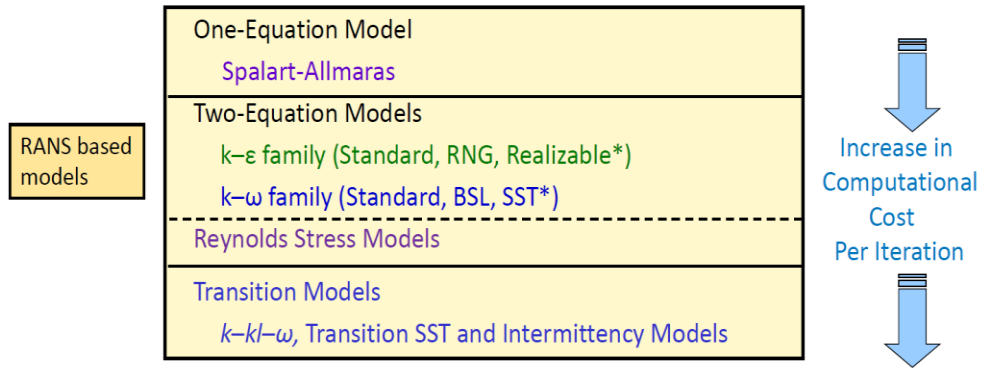


Fig. 2.20

Some are used for very particular applications.

SST $k-\omega$ and Realizable $k-\epsilon$ are recommended choices for standard cases. In this study SST $k-\omega$ model has been adopted. Usually the $k-\omega$ is used to resolve critical boundary layers, then if just a simple estimate of turbulence is requested, the standard $k-\epsilon$ can be fine.

Regardless of the type of turbulence standard parameters can be used like:

- default turbulent intensity value of 5%;
- for internal flows, turbulent viscosity ratio of 10-100 is typically good.

Chapter 2.6: Mesh setup.

Ansys offers the possibility to perform a global meshing automatically without intervening locally. The tool provides the most appropriate meshing based on the complexity of the geometry looking for a compromise between accuracy of the meshing and quality of the meshes.

At the end the tetrahedral or hybrid grid is converted into polyhedral.

Polyhedral meshes are considered the most suitable for a CFD simulation for several reasons:

- better quality;
- they reduce cell count;
- more control of the conversion by the user.

A picture of the differences between the polyhedral meshes and hybrid ones is shown in fig 2.21. It is very important to highlight that a particular attention must be paid for the boundary meshes in proximity of the walls. Since the CFD is very sensitive to the slip effect of the wall due to the viscosity of the fluid, by increasing the number of boundary layers close to the wall is possible to

improve the mesh quality and also the simulation results. The number of layer, in fact, not only can affect the orthogonal quality but also the Y^+ value, the vital of importance for a proper calculation.

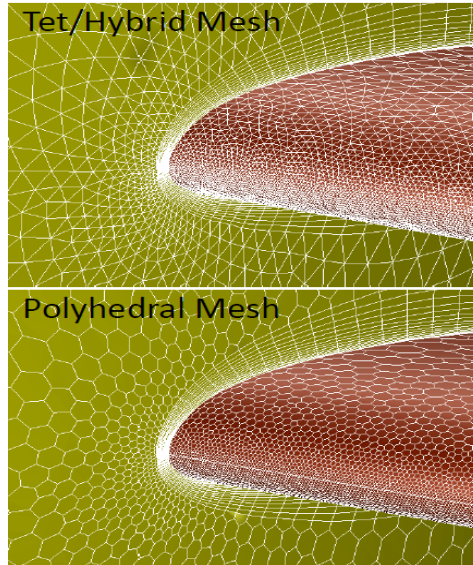


Fig. 2.21 Comparison between Hybrid and Polyhedral Mesh.

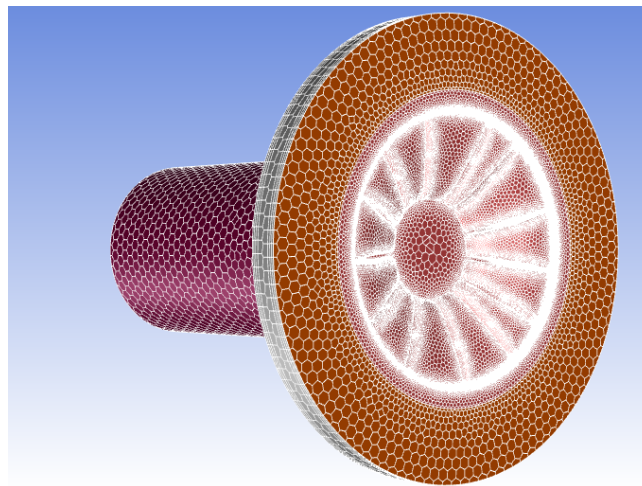


Fig. 2.24 Mesh results of the fan model.

Chapter 2.6: Fluid velocity results.

In this paragraph the results of the CFD simulation related to the fan model are presented. The calculation results are illustrated in terms of fan curves and velocity field distribution, since they represent the scope of this initial model. Several simulations are run with the aim to calculate the

pressure drop caused by the presence of the fan. This model including only the radial cooling fan will be later included in the whole model of the traction motor, for reason is very important to understand if the 3D model is working properly in order to reproduce the correct behavior of the real fan. The simulations are computed for different speeds that a reasonably close to the angular velocities of the motor applications. In fact, the fan is shaft-mounted and consequently it will rotate always at the same speed of the rotor. Since one of the boundaries of the model is set as *mass-flow inlet*, the mass flow rate represents an independent output of the system. For this purpose, a range of mass flow rate values between 0.3 and 1.2 kg/s is taken into account in order to keep the work point away from the stall region, where the fan would start working with a non-feasible physics.

The first simulations is carried out at 2500 rpm rotational speed and with a number of iterations equal to 300. Since the model is very simple because the geometry has been simplified as much as possible and cleared of all the fan details in order to take into account only the aspects important from the fluid-dynamic point of view, it results in improving of the computational cost. In fact, with a simulation time of just 740.529 seconds it has been possible to conduct the calculation the convergency. The fan curve obtained is shown in Fig. 2.25.

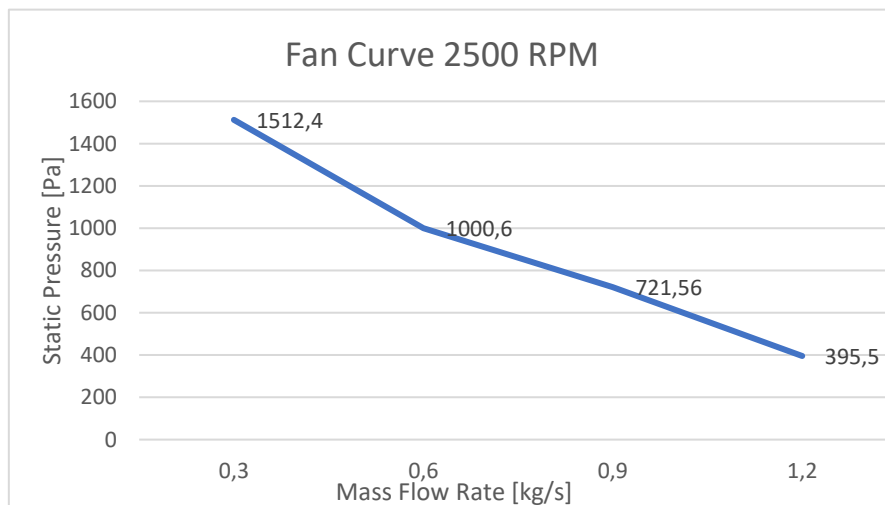


Fig. 2.25 Fan Curve of the cooling fan obtained from the simulation at 2500 rpm

Since one of the boundaries is represented by a pressure outlet and the pressure is set constant to zero, measuring for each mass flow rate input the pressure at the outlet, this value of pressure will be exactly equal to the Static Pressure.

The second simulation is run with the same mass flow rate range, since the fan is always the same, but this time the motor speed is set at 2000 rpm. The number of iterations completed is 300 and the simulation time is 710.479 seconds. The calculated chart is shown in Fig. 2.26.

The same happens for the design of the third fan curve calculated at 1500 rpm, with 300 iterations in 687.934 seconds.

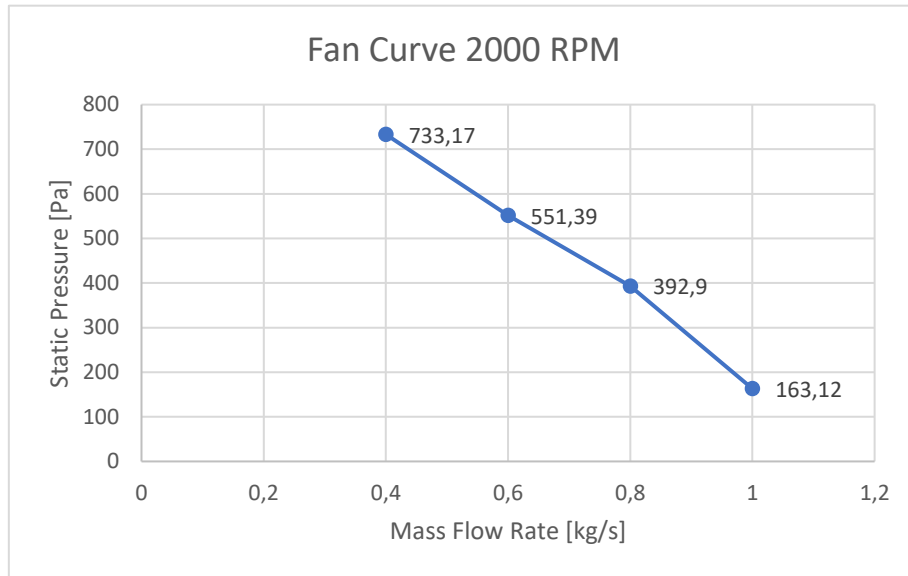


Fig. 2.26 Fan Curve of the cooling fan obtained from the simulation at 2000 rpm

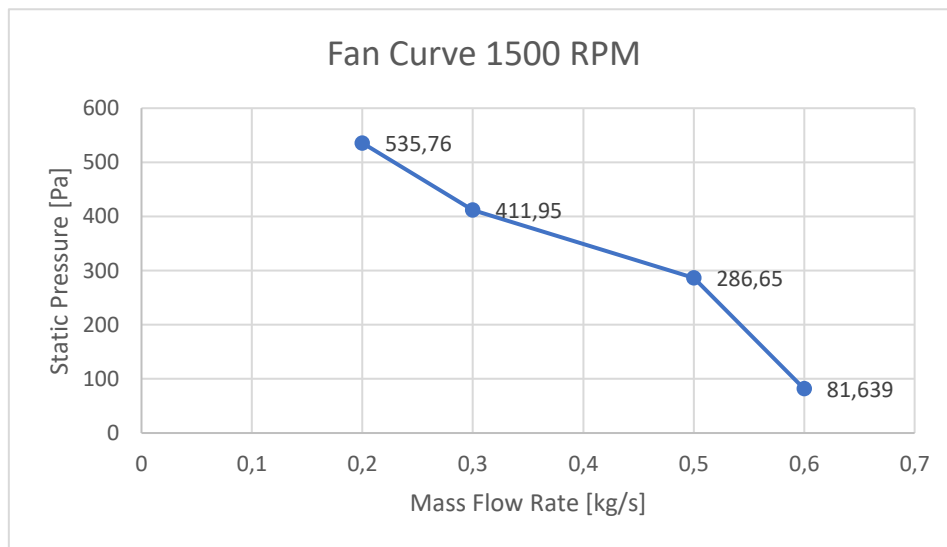


Fig. 2.27 Fan Curve of the cooling fan obtained from the simulation at 1500 rpm

In this preliminary study is very important not only to obtain and observe the static pressure-mass flow rate curve with the aim to ensure that the fan model is working correctly, but it is interesting also to have an idea of the magnitude velocity distribution inside the cooling system. Once the previous fan curve are defined, the velocity contours for each simulation are plotted. At this level of the study, it is necessary to verify to have feasible velocity of the cooling fluid, at most near the conduct walls and the fan blades. As abovementioned, performing a good quality of the mesh of the

model is the vital if importance to create a reasonable effect in correspondence of the walls where the fluid flow should be equal to zero as shown in Fig.2.26 for the simulation in question.

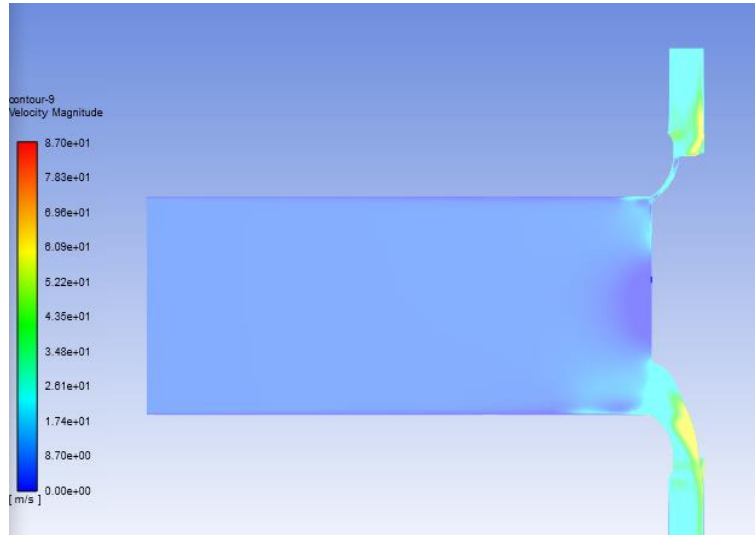


Fig. 2.28 Velocity magnitude contours at 2500 rpm and 0.6 kg/s

In addition, as shown in the figures, the maximum velocity is reached at the blades where the rotating fluid domain has the maximum tangential component.

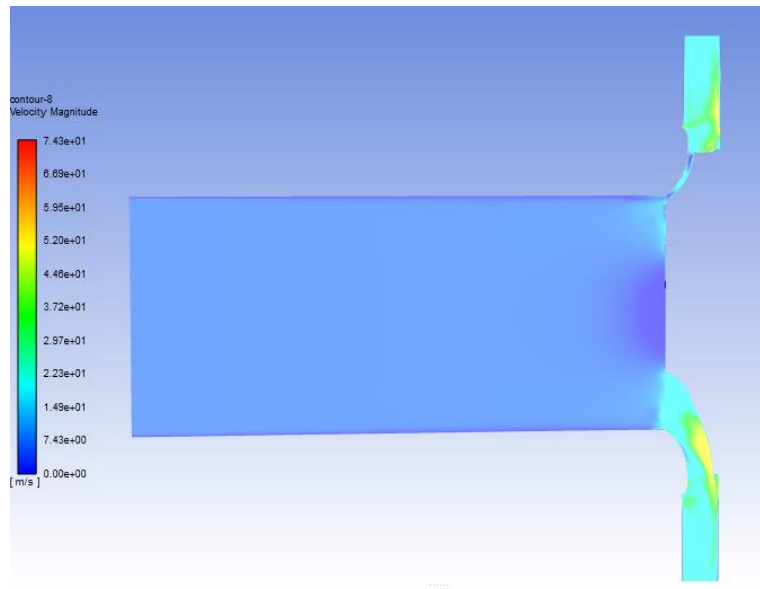


Fig.2.29 Velocity magnitude contours at 2000 rpm and 0.6 kg/s

All the contours renderings are computed with 2500, 2000 and 1500 rpm respectively and the mass flow value is set as 0,6 kg/s, value that proved to be fine for all the simulations.



Fig 2.28 Velocity Magnitude contours at 1500 rpm and 0.6 kg/s

Chapter 3: Computational Fluid Dynamics (CFD) of Traction Motors.

The aim of this chapter is to implement an accurate model in order to calculate the airflow inside the railway motor under study. For this purpose, only the fluid domains are considered and fast computation with an error within the range of 5% is achieved.

Chapter 3.1: Introduction: modeling challenges for Railway Motors.

Electric motors represent the most efficient system for railway traction. They are characterized by several advantages like low pollution level, broad speed control range and fast start-stop.

The design of the cooling system for traction motors strongly depends on loss distribution of all the losses in duty cycle. Since the temperature does not increase in each motor part at the same way and level, a thermal strategy is required to investigate and prevent the damage of the most critical components. The objective is to limit the temperature in some parts like end-winding, bearings and magnets since it can cause a deep reduction of the motor lifetime and performance.

Railway motors have typically high torque density and power bringing the need to provide a forced ventilation which supplies the motor with constant and clean airflow. This can lead to a better temperature control making also the motor overheating independent from its operating condition. On the other side this kind of configuration requires space for external fan and extra ducts resulting in additional encumbrance.

In this thesis, a shaft mounted fan in the self-ventilated motor is considered, where the need for ducts and roof-mounted external fan is complexly erased.

Chapter 3.2: 3D modeling of the motor cooling system.

The cooling system of the motor is modeled in SpaceClaim®.

For this aim only the components considered essential from the fluid-dynamic point of view are taken into account. For example, washers, tie rod, O-rings and all the other objects important for the mechanical seal and assembling are excluded from the study.

This is done not only to get a simplified version, but also for reducing the size of the model and consequently the number of generated cells of the mesh in order to make the computation easier and much faster. It is well known, in fact, that the inserting of a large number of details unnecessary from the thermal point of view, can results in an increase of the amount of work for the meshing and in a higher probability to get into errors.

For all the abovementioned considerations, the geometry shown in Fig. 3.1 is realized.

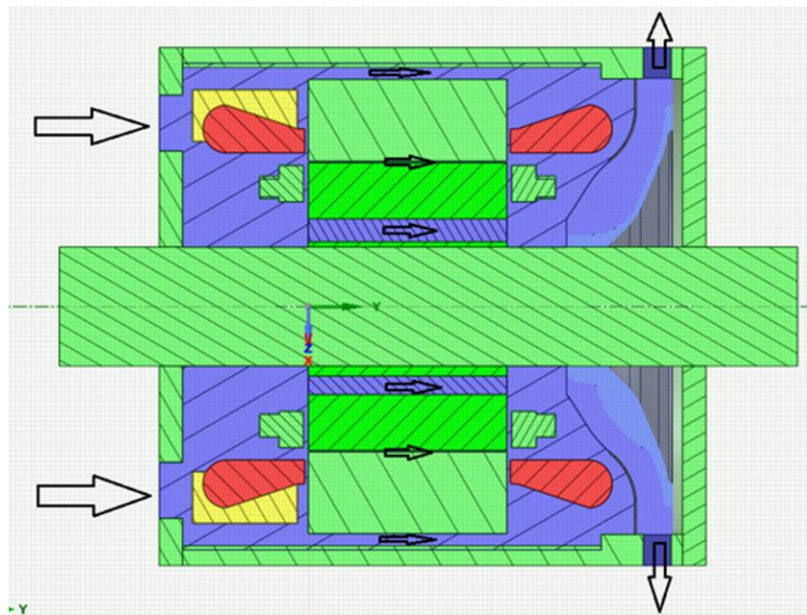


Fig. 3. 1 Cross-sectional view of the motor modeled in SpaceClaim.

The cooling system of the case study motor consists of a shaft mounted radial fan, stator ducts, rotor ducts and air gap.

The fan sucks the coolant, in this case the air, through the inlets and along the ducts in order to promote the convection thermal exchange. Then, the air is expelled outside the motor through the radial inlets machined in the external housing of the motor.

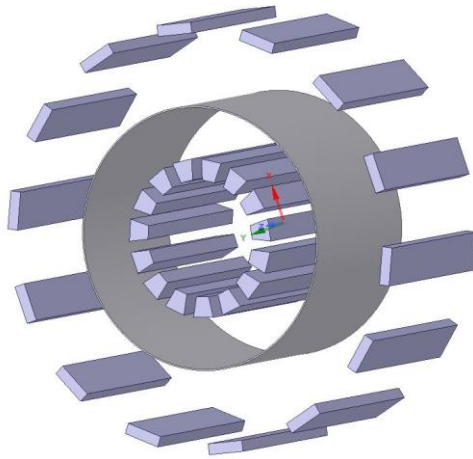
The black arrows show the direction of the airflow along the axial direction from a cross-sectional view. As can be seen, also the air valve applied on the short circuit ring have a key role in the cooling of the machine together with the ventilation effect of the whole rotor.

Once all the solid components are designed, the fluid domains inside the motor are extracted and with the aim to implement the fan, the model built and validated in Chapter 2 is inserted.

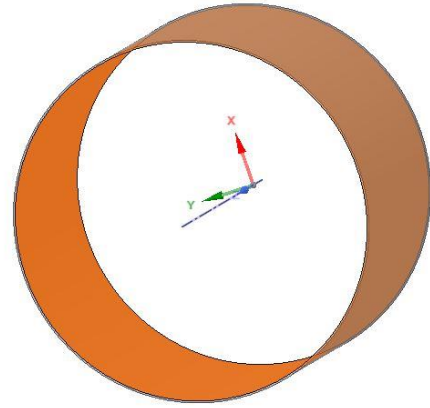
For having an idea of all the fluids at stake, the in Fig. 3.2.a all the domains involved are shown.

It is important to stress that, at this level of the study, not to consider the solids does not affect the results. It is of vital importance, on the other hand, to take into consideration the rotor speed, putting in rotation the fluids inside the rotor ducts and the airgap. For the latter, it is enough putting in rotation the inner surface of the airgap domain touching the rotor as shown in Fig. 3.2.b since even the airgap, albeit to a lesser extent, contribute to the cooling. In Fig. 3.2.b the fluid domain of the airgap is illustrated. In red it is evidenced the wall where the boundary conditions are applied. As explained in the following paragraphs, the rotation of this wall will not affect to a large extent the results, but it is considered because it slightly improves the rotor and stator cooling, although the most is surely provided from the ducts.

Another consideration can be done regarding the heat that the motor exchange for convection with the external ambient.



a) All the domains inside the ducts and airgap



b) Airgap wall put in rotation

Fig. 3.3 Fluid domains extracted

With the aim to simulate the surrounding environment and provide free boundary conditions to the motor inlets and outlets, a big enclosure is built as shown in Fig. 3.3. In this case, the usual practice is that we have an enclosure four or five times the motor dimension in order to create laminar airflow at the motor inlets and not to have any kind of turbulence caused by the enclosure boundary conditions.

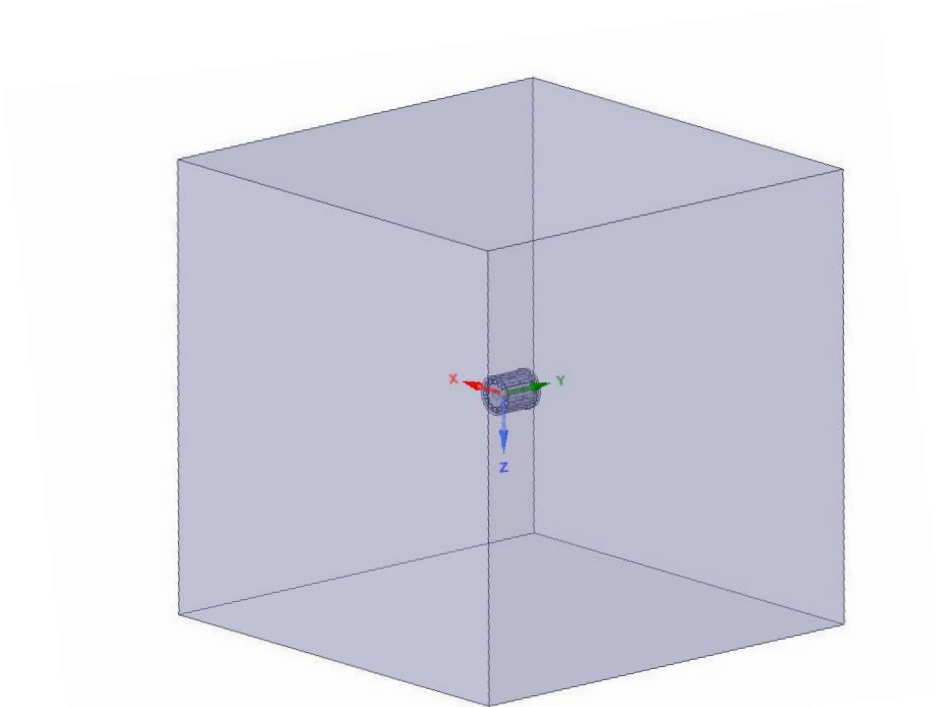


Fig. 3.2 The motor fluid domains.

Chapter 3.3: Boundary conditions and solver setup.

The following boundary conditions are applied to the enclosure:

- **Pressure inlet** at the enclosure entrance. This is used to define a free inlet in an unconfined environment.
- **Pressure outlet** at the enclosure exit. This is also useful to define a generic pressure leaving the boundary free.
- **Symmetry** at the other sides of the enclosure. This allows to have zero normal velocity and zero normal gradients for each variable at the symmetry surfaces.

The following boundary conditions are applied to the fluid domains:

- Air gap inner wall (Fig. 3.2.b) is set as rotating wall at the rotor speed.
- In the same way of the air gap, also the air valves on the short circuit ring are rotated.
- For the fluid domain inside the rotor ducts the *frame motion* is applied.
- The rotating fan fluid is set as illustrated in Chapter 2.
- The air guide is put into rotation with zero speed and *absolute frame motion*. In so doing, the fluid closest to air guide wall is very low relative to the fan speed.

Regarding the solver setup, SST k- ω model is employed as shown in Fig.3.4. This with the aim to model:

- A gradual transition from the standard k- ω model at the inner boundary layers to a k- ϵ model with a high Reynolds number at the outer boundary layers.
- The modifications to the viscosity formulation to take into account the transport effects due to the shear-stress.

Additionally, a pseudo-transient calculation is activated. It allows to give more stability to the simulation, and, at the same time, it increases the convergence chance when a steady-state computation is running. Pseudo-transient can be considered like an implicit under-relaxation form. The relaxation factor is represented by the pseudo-time-step Δt can be chosen to improve the convergency.

Since only the airflow and convection factor are estimated at this stage of our study, the energy is not activated and the heat transfer not taken into consideration.

Solution Methods

Pressure-Velocity Coupling

Scheme

Coupled

Spatial Discretization

Gradient

Least Squares Cell Based

Pressure

Second Order

Momentum

Second Order Upwind

Turbulent Kinetic Energy

First Order Upwind

Specific Dissipation Rate

First Order Upwind

Transient Formulation

☐ Non-Iterative Time Advancement
☐ Frozen Flux Formulation
☒ Pseudo Transient
☒ Warped-Face Gradient Correction
☐ High Order Term Relaxation

Options...

Default

Viscous Model

Model

☐ Inviscid
☐ Laminar
☐ Spalart-Allmaras (1 eqn)
☐ k-epsilon (2 eqn)
☒ k-omega (2 eqn)
☐ Transition k-kl-omega (3 eqn)
☐ Transition SST (4 eqn)
☐ Reynolds Stress (7 eqn)
☐ Scale-Adaptive Simulation (SAS)
☐ Detached Eddy Simulation (DES)
☐ Large Eddy Simulation (LES)

k-omega Model

☐ Standard
☐ GEKO
☐ BSL
☒ SST

k-omega Options

☐ Low-Re Corrections

Options

☐ Curvature Correction
☐ Production Kato-Launder
☒ Production Limiter
☐ Intermittency Transition Model

Model Constants

Alpha*_inf

1

Alpha_inf

0.52

Beta*_inf

0.09

a1

0.31

Beta_i (Inner)

0.075

Beta_i (Outer)

0.0828

TKE (Inner) Prandtl #

1.176

TKE (Outer) Prandtl #

1

SDR (inner) Prandtl #

2

SDR (Outer) Prandtl #

...

User-Defined Functions

Turbulent Viscosity

none

Fig. 3. 4 Solver setup

Chapter 3.2: Mesh setup.

For the CFD calculation all the fluids are imported and meshed as shown in Fig. 3.5.

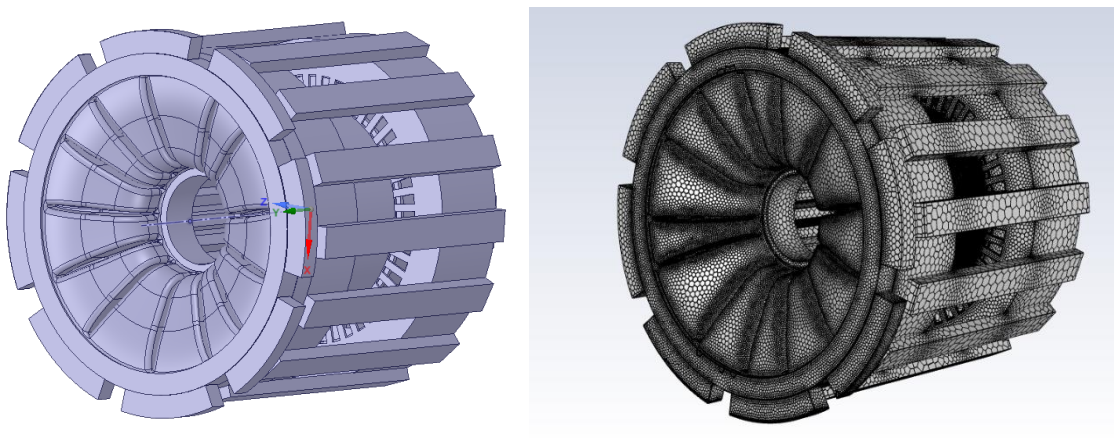


Fig. 3. 5 Fluid domains import and meshing.

The meshing method adopted is the Mosaic Meshing Technology.

Simulation time and accuracy are critical concerns in CFD computations, and both are strictly dependent on the properties of the meshes. Sometime different type of meshes are required to model challenging geometries and particular fluid regimes. In addition, the transition from a type to another one has always been hard to realize because of the interface zones where non-conformal meshes are needed creating problems about mesh quality and excessive number of cells. The aim is therefore to minimize the mesh transitions by mixing usual mesh types.

Chapter 3.2: CFD Results

In this paragraph the CFD resulting from the simulation are shown.

The size of the model is relatively low with the number of cells equal to 2963166.

The simulation is run at 3000 rpm and the contours of the airflow velocity magnitude are illustrated in Fig. 3.6 and Fig. 3.7 along the radial and axial directions.

In addition, in Fig. 3.8, the pathlines of the velocity magnitude of the fluid domains inside the motor are shown. In this case, the fan is proved to work properly since it can suck the air in the ducts and

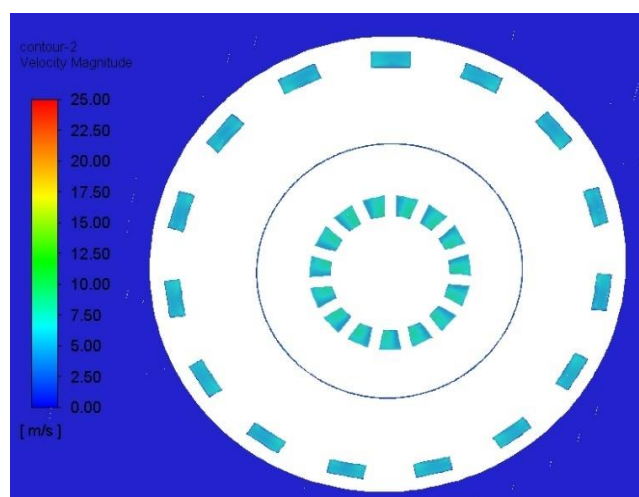


Fig. 3. 6 Airflow velocity magnitude along the radial direction.

expel it from the outlets. As the rotating components are the rotor ducts, the fan and the outer surface of the rotor, it is correct to find in proximity of them the maximum velocity magnitude in green and red how displayed in the contours.

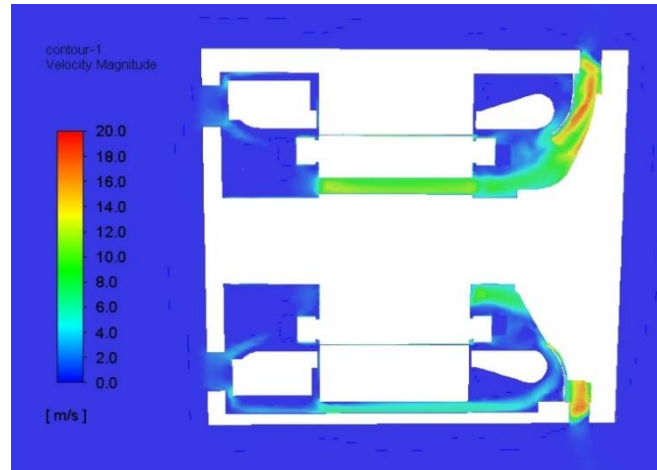


Fig. 3. 7 Airflow velocity magnitude along the axial direction.

By parametrizing the motor speed and, in so doing, also the fan speed since it should be reminded that the fan is shaft-mounted, it is possible to plot the trend of the mass flow rate in function of the motor speed. The mass flow rate considered is indifferently the one at inlets or outlets since from the computation they appear to be the same and this is true from the law of conservation of mass.

Obviously, the mass flow rate increases with the speed of the fan and is directly proportional to it.

This evaluation will be validated with an experimental setup demonstrating the high accuracy of the model.

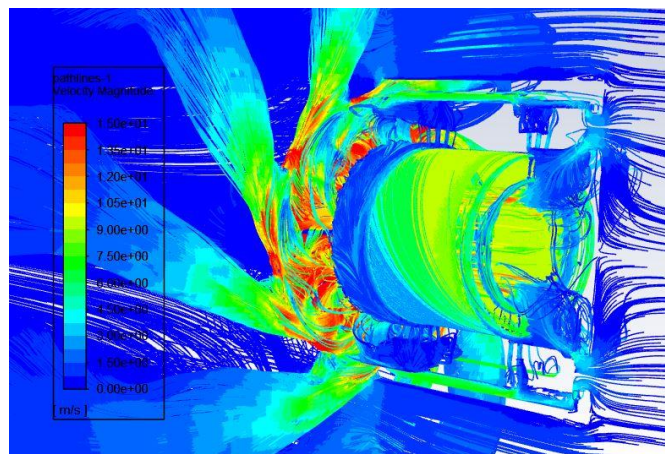


Fig. 3. 8 Path lines of the fluid velocity magnitude inside the motor.

It should be highlighted that one of the merits of this CFD model is the very short computation time. For each design point, at a particular speed, the simulation takes less that 10 minutes to get the convergency instead of hours.

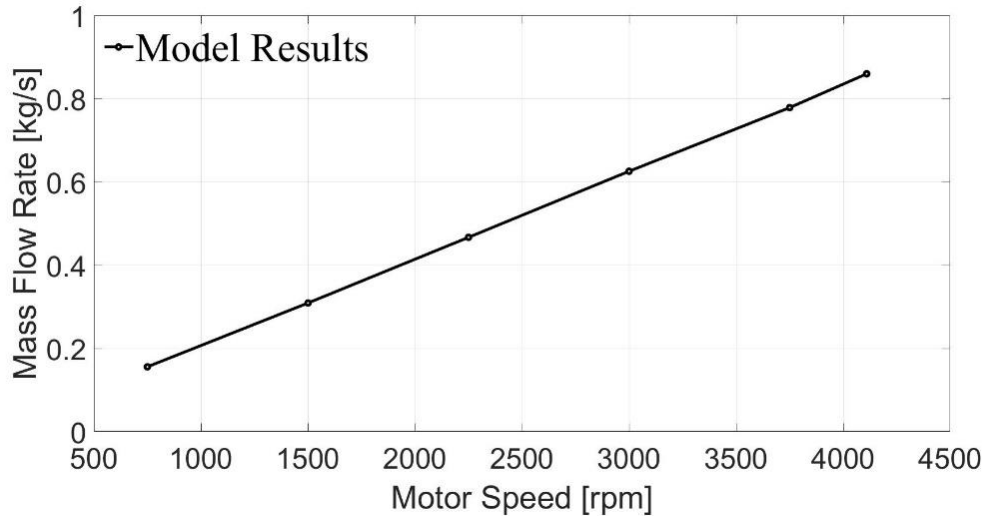


Fig. 3. 9 Mass flow rates in function of the motor speed

Chapter 4: Conjugate Heat Transfer Model (CHT).

Once the CFD analysis is concluded, a thermal simulation is conducted in order to predict the thermal behavior of the machine with high accuracy. For this aim, all the solid components are now included in the physic and the energy is activated. One of the key objectives of the analysis is to find an adequate method to model critical parts of the electrical machines thermal design like end windings and stator slots.

Chapter 4.1: Most difficult aspects of electrical machines thermal modeling.

The need of fast and compact computations able to simulate at the same time fluid dynamic and thermal behavior has triggered the development of Conjugate Heat Transfer models.

The acronym CHT indicates a numerical method where computation fluid dynamic and heat transfer are activated at the same time. With the more common analytical approaches, the thermal network is built by incorporating convective heat transfer coefficients from a calculation apart. This takes not only to a low accuracy since most of analytical formula deeply approximate the complex geometry of electrical machines, but it also makes the model less compact and parametrizable.

With a correct CFD is in fact possible to simulate also the convection phenomena around the end-windings, and the effects of turbulences between end-shield and lamination that would otherwise not be taken into consideration.

Another advantage is also represented by the chance to consider the fluid density variation in function of the temperature of the coolant: in case of traction motor, the temperature may notable increases changing the properties of the fluid used for the cooling system. For this purpose, it is possible to parametrize the density in order to make it temperature sensitive. For all this reasons and others, CFD and HT (heat transfer) are strongly interconnected.

Despite all the benefits of the numerical methods, the thermal modeling of electrical machines can be very challenging. The most critical parts are surely represented by the stator slots where so many elements are present very hard to model. Other difficult aspects are certainly the bearings for which a known thermal behavior does not exist because of the complexity of the system, and the thermal resistances between the various solid components whose values are closely related to the air pockets in interfaces.

Chapter 4.2: Windings and end windings model.

An efficient thermal model to predict the thermal behavior is the vital of importance since the machines parts do not increase their temperature in the same way. For example, it is usual to attribute the largest temperature increase to the windings and end windings, and a valid prediction is fundamental in order to impose temperature limits.

In the electrical machines, the slots represent surely the most critical part from the thermal modeling point of view since there are random factors due to the position of the conductors (especially for random-wound windings) and air pockets depending on the fill factor and quality of impregnations. In addition, also the number of the conductors and the type of insulation can be predominant factors and defining a thermal network by calculating analytically all the parameters can be not easy and not feasible.

Simplified strategies are employed keeping the analysis within a high accuracy range. For this aim, several approaches based on analytical, experimental and finite element methods are illustrated. Each of them can be regarded as a valid way for modeling the stator slots of electrical machinery, but they have advantages and disadvantages depending on the case that are explained as following.

4.2.1 Finite Element Method.

A detailed 3D geometry of the stator slots is designed taking into consideration only the relevant parts that can influence the temperature. A simplified version of the stator winding is displayed in Fig. 4.1 and Fig. 4.2.

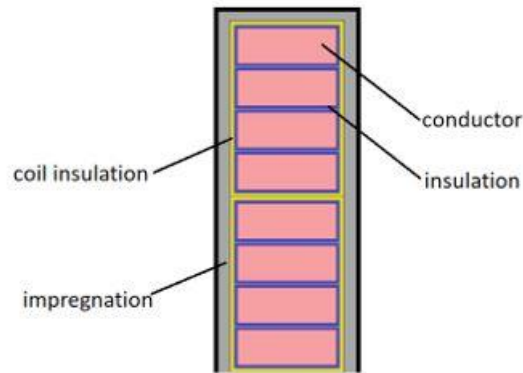


Fig. 4. 1 Stator slot structure

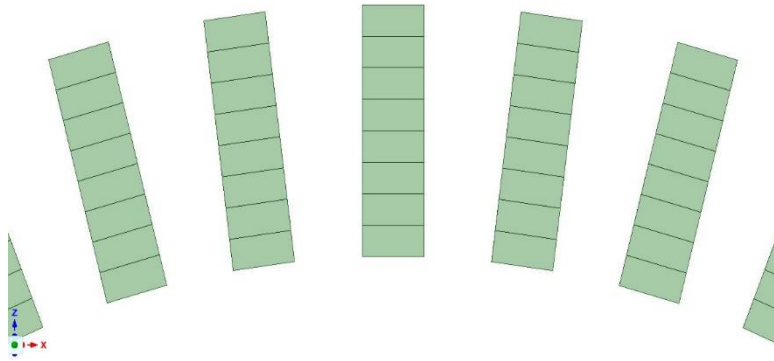


Fig. 4. 2 Geometry design of stator windings in SpaceClaim.

In the thesis case study, there are form-wound windings characterized by two coils and each coil consists of four conductors. The stator slot is formed by eight conductors overall. Although this system may be considered easily implementable, it requests the knowledge of several data like the conductors dimensions, conductors disposition (in the case of random-wound windings the exact location of the conductors is very aleatory) and insulation and impregnation thermal parameters, that makes this method, sometimes, not simple to realize.

In this thesis, FEM is adopted, seeing as the stator has form-wound windings reducing the complications.

Inside the stator slots many elements exist and, from the thermal point of view, this means more resistances and capacitances. *Shell Conductions* are needed to model the thermal resistances due to the conductors insulation, the coils insulation and air pockets created by impregnation imperfections.

Ansys, as default, considers borders as zero thickness walls without any thermal resistance, not affecting in any way the heat transfer. For these reasons, it is possible to locate these layers between the conductors and lamination in order to generate all the thermal resistances along the radial direction. On the other hand, the thermal resistance along the axial direction is already created by setting the copper as material of the conductors. In Table IV.I all the data inserted are listed.

TABLE IV. I
SHELL CONDUCTION SETUP

	Thermal Conductivity [W/m° C]	Shell Thickness [mm]
Conductor insulation	0.18	0.25
Coil insulation	0.20	0.50
Air pockets	0.03	0.009

4.2.2 Analytical approach based on homogenization.

The aim of this method is to calculate the thermal conductivity related to an equivalent thermal model used to simplify the complexity of the stator slots structure. Everything inside the stator slot is modeled like a single compound made of two different phases. The first one corresponds to the conductors made of copper with a thermal conductivity equal to λ_1 , the second phase of the compound represents the resin with a thermal conductivity λ_2 . This method does not consider insulated conductors since the enamel has thermal properties very similar to the impregnation.

In order to take into account the air pockets inside the resin, a preliminary equivalent compound of the insulation is computed by using the following formula (4.a).

$$\lambda_{eq} = \lambda_2 \frac{(1 + \tau_1)\lambda_1 + (1 - \tau_2)\lambda_2}{(1 - \tau_1)\lambda_1 + (1 + \tau_2)\lambda_2} \quad (4.a)$$

In this equation, τ represents the volumic ratio ($\tau_1 + \tau_2 = 1$). Considering a very well-made impregnation, the equivalent thermal conductivity of the insulation is calculated with the data in Table IV.II where only the 10% of air is considered since for the case study motor the windings are form-wound type.

Once a realistic value of the resin thermal conductivity is obtained, it is possible to use again the formula (4.a) to get the equivalent thermal conductivity of the whole stator slot. This time, λ_1 and λ_2 will stand for the copper and resin thermal conductivity respectively. The same for the volume ratio values τ_1 and τ_2 : this time a fill factor typical for electrical machines application of 0.65 is employed as shown in Table IV.II.

TABLE IV. II
INSULATION THERMAL CONDUCTIVITY

	Thermal Conductivity λ [W/m° C]	Volume Ratio τ
Resin	0.25	0.90
Air pockets	0.03	0.10
Insulation	0.17	1

TABLE IV. III
STATOR SLOT THERMAL CONDUCTIVITY

	Thermal Conductivity λ [W/m° C]	Volume Ratio τ
Copper	0.25	0.65
Insulation	0.03	0.35
Total insulation	0.17	

This model will be validated with an experimental setup based on Short Transient Test as following.

4.2.3 Experimental approach: Short Transient Test.

As previously mentioned, this experimental setup is conducted with the aim to find the thermal parameters of electrical machines windings by using laboratory measurements.

The method applied is based on Short Transient, where as the name implies, the machine is supplied with DC current and just a short time period of temperature evolution is considered so that the heat exchange between stator lamination and winding is not started yet. And it is exactly the aim of the experiment: the temperature transient must refer to the stator slot only for the evaluation of the correct parameters.

This methodology can be adopted with the objective to define values that can be implement as input in fem models, lamped approaches or as validation for analytical estimation.

The thermal network that better explains the study is the first order thermal model in Fig. 4.3

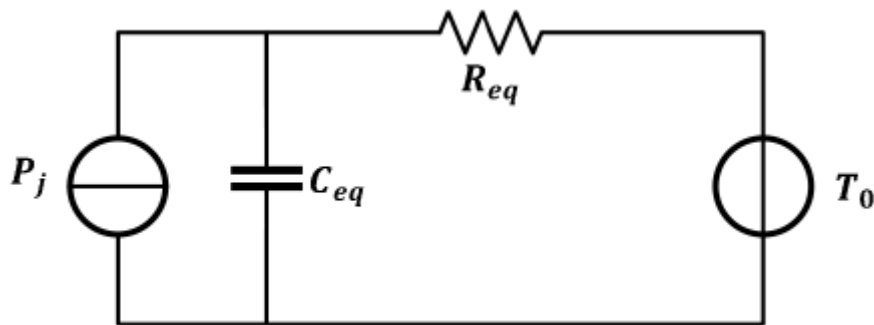


Fig 4. 3 First order thermal model.

The DC current supplier symbolizes the Joule losses of the stator windings, the R_{eq} the thermal resistance between the windings and the stator lamination and the C_{eq} the equivalent thermal capacitance of the windings united with insulation. T_0 is the initial temperature of the motor equal to room temperature.

The use of a DC current allows to:

- Localize the losses only in the stator windings (no iron and joule losses of the rotor are generated).
- Calculate the windings resistance with the ratio of the supplying voltage and current. Its variation is regulated by the well-know relation (4.b).

$$R_T = R_0 \frac{B + T}{B + T_0} \quad (4. b)$$

$$T = (B + T_0) \frac{R_T}{R_0} - B \quad (4. c)$$

In these formula T and T_0 are the winding temperatures at actual and initial instant. R_T and R_0 represent the actual and reference electrical resistances of the stator-winding. By using the (4.c) it is possible to obtain the evolution of the winding temperature.

During the test, the frame and the lamination temperature is measured by several sensors located in different parts. The transient thermal test must be performed in *short time* that corresponds to minutes for the case study motor. In addition, the current provided is of the same order of magnitude of the rated current.

At the beginning, the motor is at the room temperature and the test is performed for one hour. For the post-processing only the first 2 min of the test are used in order to avoid an increase of the stator in temperature. In this way the frame maintains a constant temperature equivalent to the ambient one and the stator lamination can be considered isothermal. Not heat exchange exists between the lamination and the windings keeping the system to the first order, since all these hypotheses implies that the other thermal capacitance except the one of the windings plus insulation do not come into play.

It should be noticed that, since the motor has star connections, the DC current is provided to a series of two phases only and samples of current and voltage are recorded with a certain time step.

This is done to compute the energy and plotting the trend of the energy in function of the winding temperature, the value of the thermal capacitance can be estimated by the slope of the curve following the (4.d).

$$C_{eq} = \frac{dW}{dT} \quad (4. d)$$

Under the previous considerations, the temperature rises with a first order evolution represented by the equation (4.e) in below:

$$T_k = T_{k-1} + (T_0 + R_{eq}P_{k-1} - T_{k-1})(1 - e^{-\frac{t_k - t_{k-1}}{R_{eq}C_{eq}}}) \quad (4. e)$$

As all the variables in the equation are known, the R_{eq} can be computed making minimum the square mean error between the temperature measured by the sensors and the one obtained from the first order evolution as follows:

$$Err = \frac{(T - T_k)^2}{T_k^2} \quad (4. f)$$

In the following sections all the measurements and results will be presented. All the data are recorded and analyzed with Yokogawa 1800 by varying the sample time to 0.1, 1 and 5 seconds respectively till the stator temperature does not exceed the variation temperature equal to 1°C considered as threshold. For the investigated motor, a sample time of 5 seconds has proved to be appropriate. As abovementioned, since the neutral point is not accessible, only two phases in series are taken into account for each test and at the end a correction factor is applied.

1) Test 1.

A sample time of 0.1 seconds is applied, and the test duration is 1 hour. In order to have correct values of V and I to use for the subsequent steps of the method, the electrical resistance calculated with the ratio between voltage and current should have the same trend of the temperature measured by the sensors in the windings, since they are directly linked through a proportionality.

In this case the too high number of samples due to a too little sampling time, led as consequence to a huge mismatch between the curves compared in Fig. 4.3 considering the first 3500 seconds.

The reasons might be found in the large size of the machines that does not allow a rapid increase of the temperature. With a little sample time there is no way to contemplate a significant increment of the temperature in a 230 kW motor. Another issue in having a very fast sampling is the risk of seeing also the electrical transient and not only the thermal one.

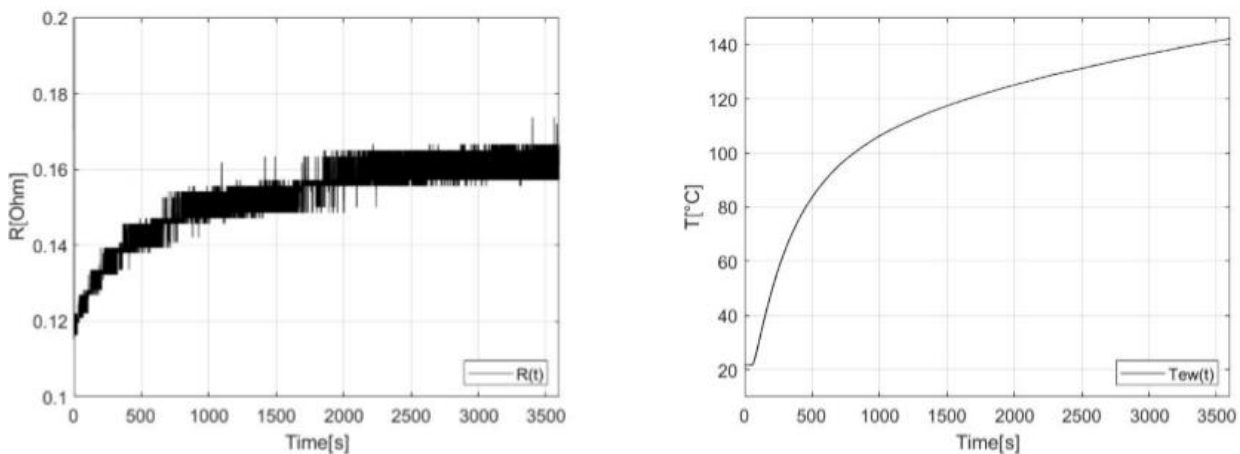


Fig 4. 4 Comparison between estimated electrical resistance and measured temperature related to Test 1

II) Test 2.

Since the results of Test 1 are not acceptable, this lead to the run of a second test.

A sample time of 1 second is applied and two different phases of the motor are put in series to respect of the previous test. In this case the trends in Fig. 4.4 show slightly better results but still with

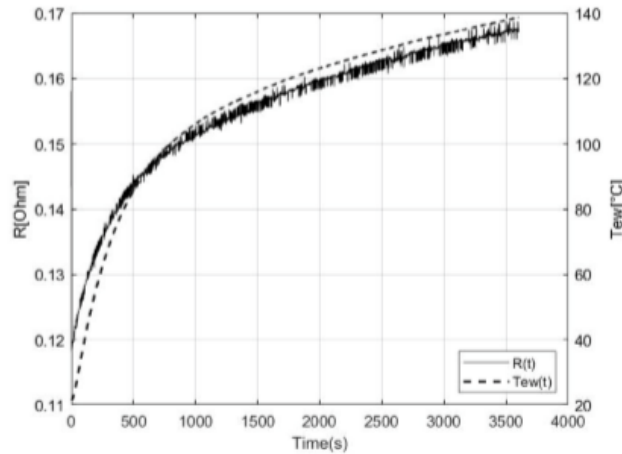


Fig 4. 5 Comparison between estimated electrical resistance and measured temperature related to Test 2

low accuracy.

With the aim to increase the accuracy of the computation, a moving average is applied to the data with a time step of 10 seconds. Using this correction, a more pseudo-linear trend is obtained showing more accurate results as shown in Fig. 4.5.

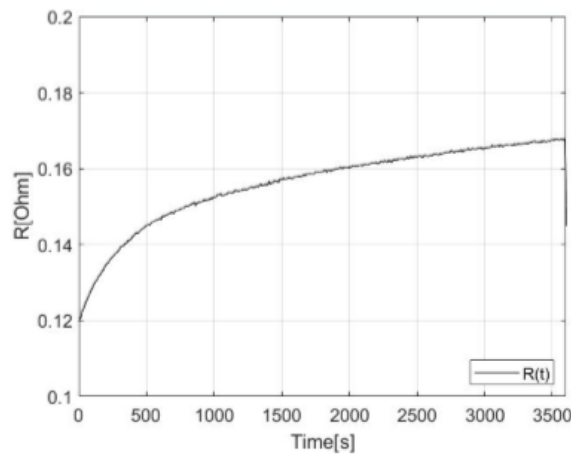


Fig. 4.6 Test 2 results filtered with a moving average.

Fig. 4.6 and Fig. 4.7 demonstrate that the accuracy of the test is guaranteed within the range of 600s , where there is a very good coincidence between the measured temperature and the one estimated with the (4.e). Also the plot of the Energy in function of the temperature variation is displayed in order to calculate the equivalent thermal capacitance from the slope.

All the voltage, current and temperature data are elaborated to calculate the thermal parameters by using the (4.d) and (4.e).

$$C_{eq} = 14393 \text{ J/K}$$

$$R_{eq} = 0.025 \text{ W/K}$$

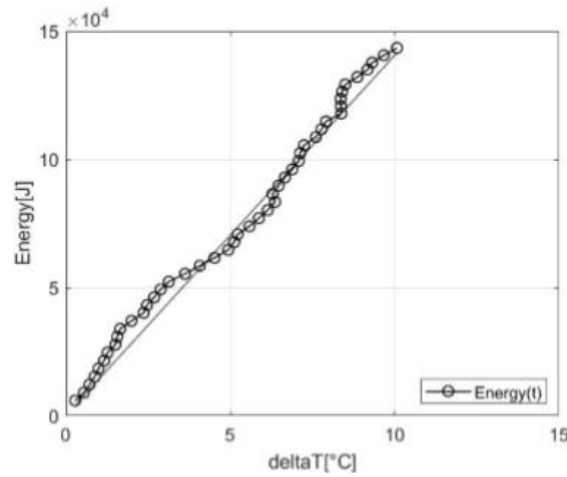


Fig 4. 7 Energy vs Temperature variation

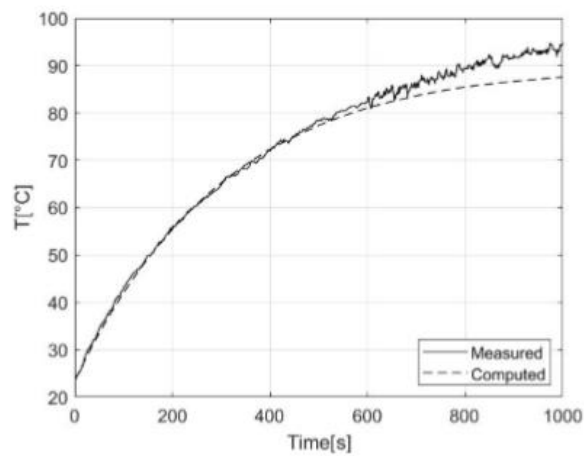


Fig 4. 8 Comparison between estimated and measured temperature related to Test 2

III) Test 3.

The last test is carried out considering a sample time of 5 seconds.

Taking into account the improvements obtained from Test 2 and with an appropriate set up, a very good agreement between the calculated and measured results is achieved as shown in Fig. 4.8.

Observing the results, it is possible to notice that the end winding temperature and the electrical resistance variation have the same trend in function of the time.

Since the objective of the study is always determine the equivalent resistance and capacitance, the computation of the energy and temperature respecting the (4.d) and (4.e) is needed, as displayed in Fig.4.10 and Fig. 4.11.

With a proper elaboration of the data, the equivalent thermal parameters of the windings are computed, and since the experimental setup considered a series of two phases only, an appropriate correction factor of 3/2 is employed.

$$C_{eq} = 16282 \text{ J/K} \rightarrow 16282(3/2) \text{ J/K} = 24423 \text{ J/K}$$

$$R_{eq} = 0.027 \text{ W/K} \rightarrow 0.027(3/2) \text{ W/K} \leq 0.018 \text{ W/K}$$

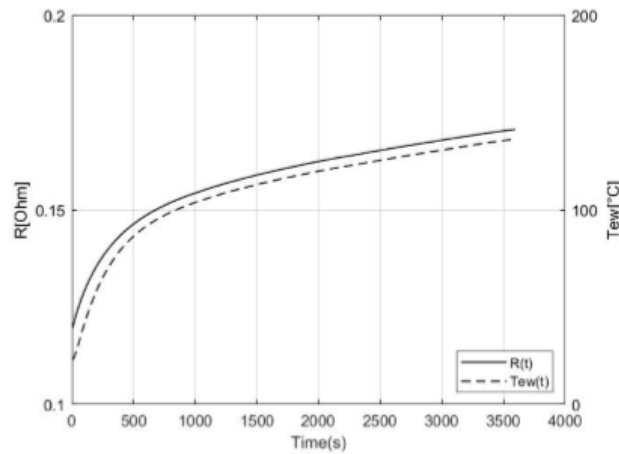


Fig 4. 9 Comparison between estimated electrical resistance and measured temperature related to Test 3

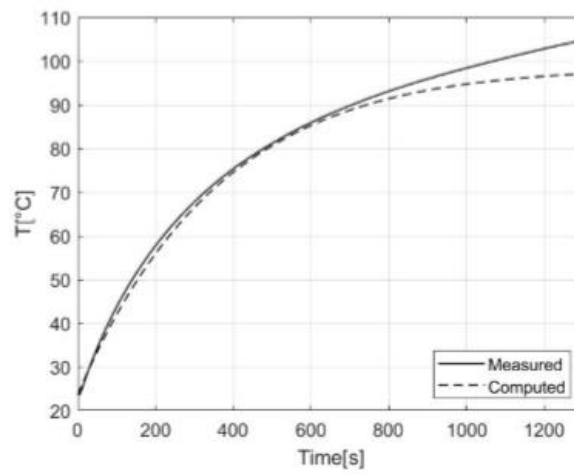


Fig 4. 10 Energy vs Temperature variation

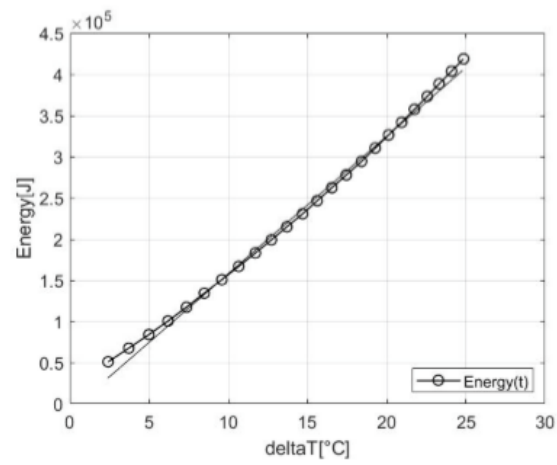


Fig 4. 11 Comparison between estimated and measured temperature related to Test 3

Chapter 4.3: Thermal resistances implementation.

For an accurate thermal prediction is the vital of importance to estimate all the thermal resistance inside the motor. Regarding the thermal resistances proper of the solids composing the electrical machine, by setting the material and designing accurately the geometries, the ANSYS tools already provide the exact values needed to simulate the correct heat transfers.

One of the most challenging aspects of the thermal design applied to electric motor is to implement the many contact thermal resistances inside the machines.

A contact resistance is created by the flaws of touching surfaces due to their smoothness, contact pressure and hardness of the materials. This leads to the creation of air pockets between the surfaces that cause barriers to the heat transfer along the solids.

The evaluation of these parameters with high precision is hard to achieve. An efficient method may consist in carrying out an experimental setup with a DC current to calibrate the thermal model.

	Interfacial Conductance [W/m ² /C]	Effective Interface Gap [mm]
Ceramic-Ceramic	500-3000	0.0087 – 0.0052
Ceramic-Metal	1500-8500	0.0031 – 0.0173
Graphite-Metal	3000-6000	0.0043 – 0.0087
Stainless-Stainless	1700-3700	0.0070 – 0.0153
Aluminum-Aluminum	2200-12000	0.0022 – 0.0012
Stainless-Aluminum	3000-4500	0.0058 – 0.0087
Iron-Aluminum	4000-40000	0.0006 – 0.0060
Copper-Copper	10000-25000	0.0010 – 0.0026

Fig 4. 12 Interfacial conductance and interface gap from Mills

	RMS Roughness [mm]	Contact Resistance [C/W]	Effective Gap [mm]
416 ground stainless (3-25atm)	0.0025	0.000264	0.0069
304 ground stainless (40-70atm)	0.0011	0.000528	0.0137
ground aluminum (12-25atm)	0.0025	0.000088	0.0023
ground aluminum (12-25atm)	0.00025	0.000018	0.0005
ground copper (12-200atm)	0.0013	0.000007	0.0002
milled copper (10-50atm)	0.0038	0.000018	0.0005

Fig 4. 13 Interfacial conductance and interface gap from Hollman

In this thesis, values considered reliable from the literature are adopted since they come from the experience and result from studies based on the material properties analysis.

The simplest way to model interface thermal resistances is to base the estimation on average interface gap values. Mills (Fig. 4.11) and Hollman (Fig. 4.12) provide valid inputs for a thermal design program to be expected between well-known materials. The given data can be easily switched to equivalent air gaps by employing the thermal conductivity of the air equal to 0.026 W/m/C. For applications typical of electrical machines the values are in the range of 0.0005 to 0.0025 mm for aluminum-aluminum interface gap , 0.007 to 0.015 mm for stainless-stainless and 0.0006 to 0.006 mm for aluminum-iron. These values can be employed for a first estimation of interface gaps for electric motors in ANSYS as illustrates in Table IV.IV.

TABLE IV. III
INTERFACE GAP WITHIN THE MOTOR

Interface	Air pockets thermal conductivity [W/m°C]	Effective Interface Gap [mm]
Housing-Stator Lamination	0.026	0.005
Stator-End Shield		
Rotor-Shaft		
Rotor Bars-Rotor Lamination		
Bearing	0.026	0.4
Windings-Stator Lamination	0.026	0.09

Chapter 4.4: Heat sources and material settings.

Thanks to a previous evaluation of the losses produced in the motor parts by the use of a corporative software, it is possible to insert the heat sources as shown in Table IV.V.

As illustrated, the yoke and teeth of the rotor and stator are considered separately in order to remain as faithful as possible to the losses of the real machine. This is possible by dividing the geometry in SpaceClaim.

In order to correctly model thermal performance of traction motor, a distinction must be made between materials with isotropic and anisotropic properties. Components, e.g. the end shield, housing, fan, conductors, bearing and insulation can be easily considered isotropic with a constant thermal conductivity in any direction as illustrated in Table IV.VI.

Concerning the stator and the rotor, anisotropic thermal conductivities have been applied in order to take the effects of the lamination into consideration. For this purpose, 10 W/m·K and 30 W/m·K have been set along the radial and axial directions respectively. Additionally, an orthotropic thermal conductivity is employed for the end windings. In this case, two values of 3.90 W/m·K and 10.54 W/m·K in the radial and axial directions respectively have been used. These values arise from the following formulae (4.g) and (4.h) considering geometry dimensions of the end windings.

$$k_{axial} = 0.15 l_{axial} \frac{1}{2.44} \quad (4.g)$$

$$k_{radial} = 0.15 l_{radial} \frac{1}{0.84} \quad (4.h)$$

Where:

- l_{axial} is the distance between the end winding center to the end winding outer surface along the axial direction.
- l_{radial} is the distance between the end winding center to the end winding outer surface along the radial direction.

These two lengths are estimated by dividing the distances sketched in Fig. 4.11 by two.

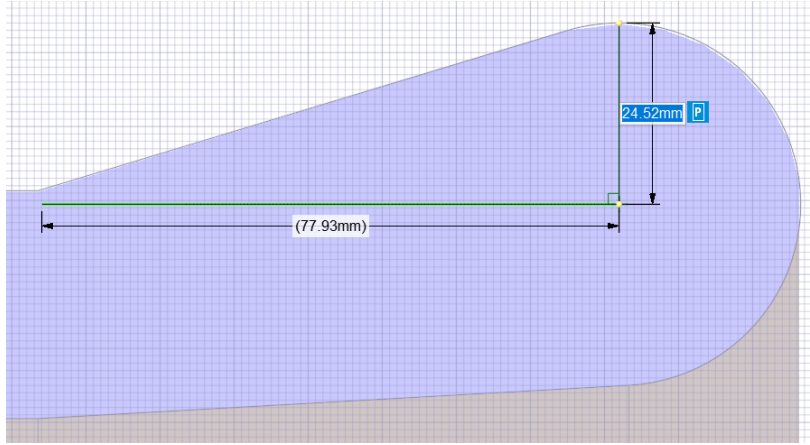


Fig 4. 24 Dividing by two the traced lengths is possible to estimate properly l_{axial} and l_{radial} .

TABLE IV. V
HEAT SOURCES

Location	Losses [W]
Stator teeth	799
Stator yoke	1815
Rotor teeth	1016
Rotor yoke	0
Friction	985
Stator winding	8513
Rotor cage	5845
Additional	2738
Total	21711

TABLE IV. VI
ISOTROPIC MATERIAL SETTING

	Thermal Conductivity [W/m °C]	Specific Heat [J/kg °C]	Density [kg/m ³]
Housing	168	833	2790
End Shield	168	833	2790
Fan	168	833	2790
Shaft	52	460	7800
Copper	401	385	8933
Insulation	0.2	1700	1400
Bearing	30	460	7800

Chapter 4.5: Steady-state thermal results.

The main achievement of this model is the ability to accurately simulate the CFD and Thermal behavior at the same time. The intention of the authors is to show in this section the results of one simulation conducted with the CHT model in less than 10 minutes with a usual laptop of 16 Gb of RAM and 2.3 GHz processor. These results will be successful validate with both airflow and thermal experimental measurements in last chapter of the thesis.

Activating the energy function in the CHT model, the distribution of temperature can be visualized in Fig. 4.13 and Fig. 4.14. It should be highlighted that the thermal results are referred to a steady state condition and do not need any analytical estimation of the convective coefficients: one of the main advantages of CHT strategy presented in this paper is that the CFD results are directly imported to the thermal module. The solution obtained in this steady state calculation is compared with the experimental measurements in the Chapter 6.

Since the case study machine is an induction motor, it is evident that the maximum temperature is reached along the rotor bars due to the internal position and the high current density. On the other hand, the temperature in the iron cores is fairly lower due to the effects of the rotor and stator ducts

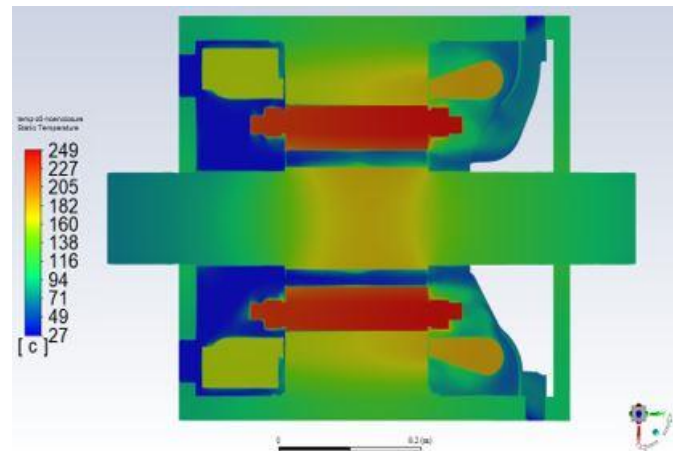


Fig 4. 15 Cross-sectional view along the axial direction of the temperature distribution contours

that properly cool down the motor. A smaller influence is instead represented by the ventilation effect of the airgap which is put in rotation to take into account the rotor rotation at 3000 rpm for this simulation.

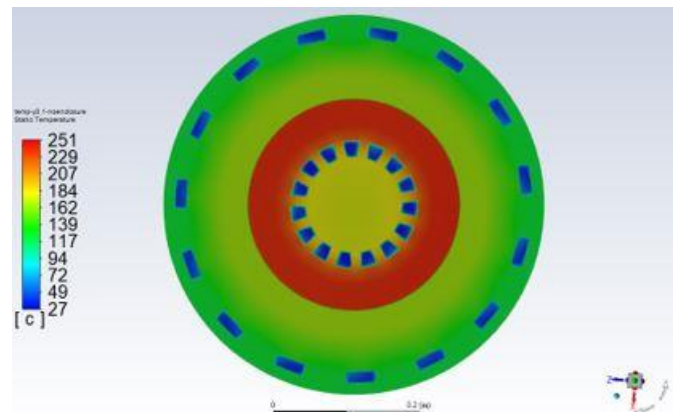


Fig 4. 16 Cross-sectional view along the radial direction of the temperature distribution contours

The hottest bodies of the motor are surely represented by the rotor bars and stator windings, since they are conductive elements where the major losses of the motor are applied.

In the picture is clearly visible the effect of the cooling fan at the non-drive-end side for both the bars and the windings. The latter is characterized also by the protrusions mounted on the short circuit ring what nurtures the creation of turbulences capable of cool the squirrel cage ends down.

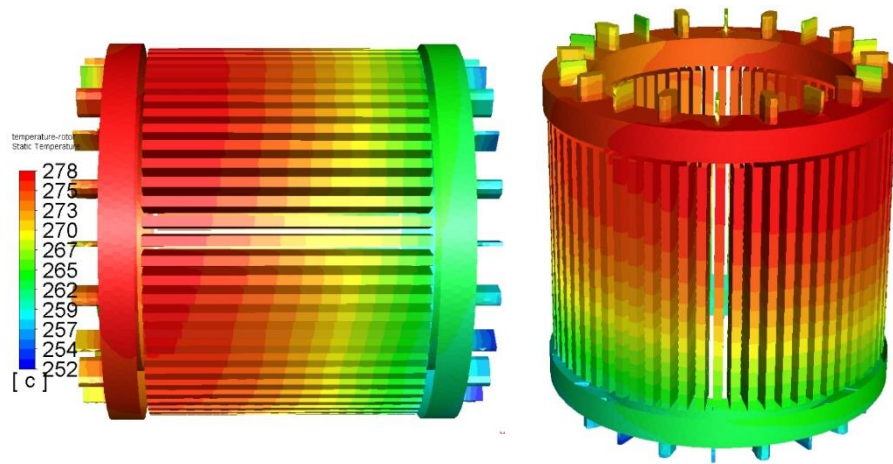


Figure 4.17 Temperature contours of the squirrel-cage rotor.

It is interesting to notice how the distribution of temperature changes in respect of the *Shell Conductions* applied to the end windings of the stator. Since they allow to increase the thermal resistance along the axial and radial direction, it results in an in a rise of the temperature in the final part of the conductors that turn out with a much higher temperature compared to the conductors of the active length.

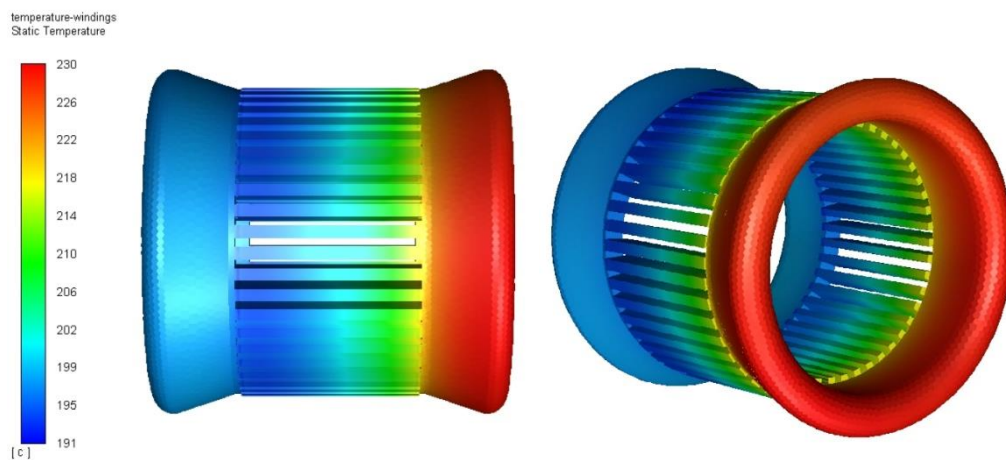


Figure 4.18 Temperature contours of the windings.

In the induction motors, one of the hot spots really hard to cool are certainly the stator slots and end windings. The results of this simulation show that the axial shaft-mounted fan can provide enough coolant to these hot spots in order to prevent conductors failures.

More specifically, we can observe the distribution of the temperature inside the stator slots that represent the most common weak point of most of the thermal design and temperature evaluations.

Since a lot of elements are inside the stator slot (e.g. conductors, insulants, resin), forecasting the temperature distribution with an accurate model is not simple.

As explained in the previous paragraphs, a good method is to implement several *Shell Conductions* to simulate the thermal resistances due to the coils and conductors insulations and the airgap between them and inside the impregnation. The values of these resistance can be evaluated with high accuracy respecting one of the methods previously presented.

The effect of the *Shell Conductions* inside the stator slots can be seen in figure were a clear variation of the distribution temperature along the radial direction is visible.

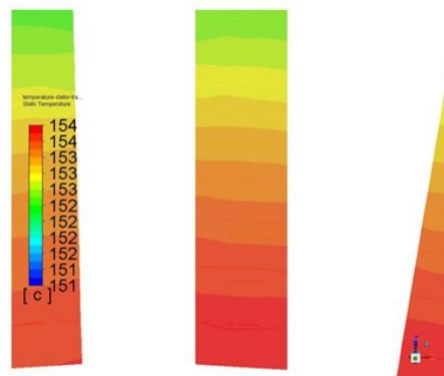


Figure 4.19 Temperature distribution inside the stator slots.

Worth of interest is also to see the temperature results in stator and iron cores.

As abovementioned in the previous chapters, for the estimation of the temperature in the motor iron, both the iron losses and lamination are considered. The iron losses are simply charged as input in the elements properties whereas the lamination is implemented inserting anisotropic thermal conductivities along the radial and axial direction. Since the lamination represent a barrier that obstacles the heat transfer, the axial thermal conductivity will be greater than the axial one.

The effects of this settings are clearly visible looking at the temperature distribution contours of the rotor and stator iron.

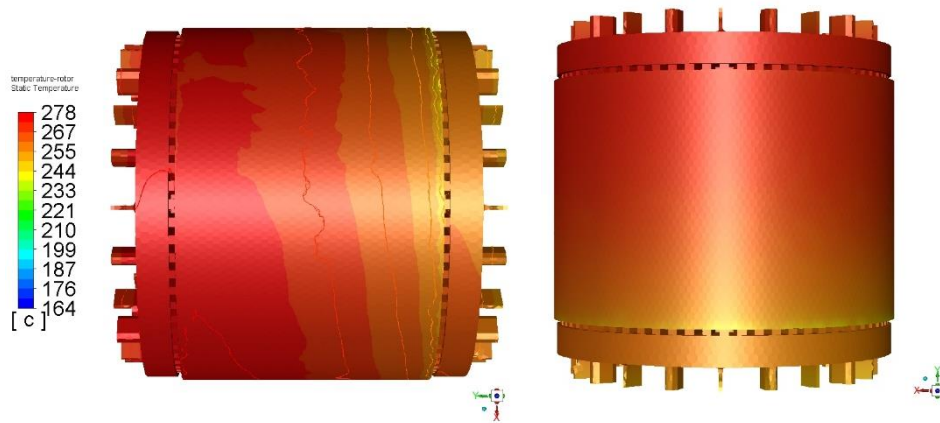


Figure 4.20 Temperature contours of the rotor core.

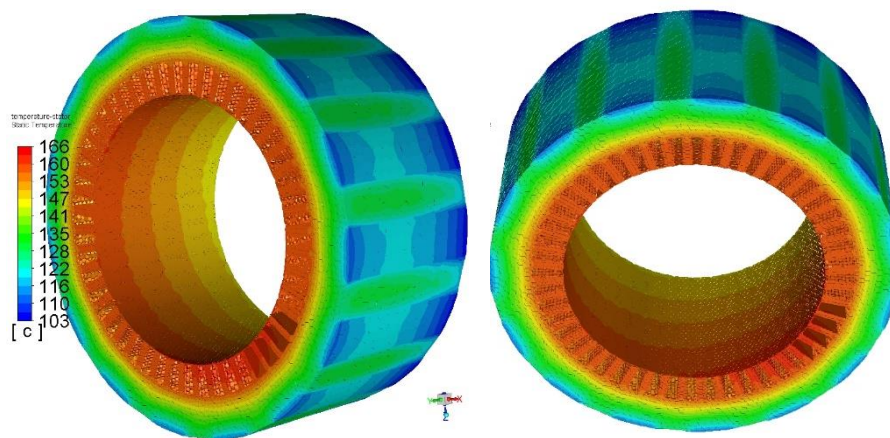


Figure 4.21 Temperature contours of the stator core.

Through the insertion of several probes inside the model, it is possible to calculate the punctual value of the temperature wherever desired. In this case, as shown in Table, an evaluation is done in precise points of the motor in order to compare the values obtained from the simulation with the ones measured with PT100 sensors located in the different parts of the motors during the experimental setup.

The comparison between estimated and measured temperature is illustrated in the final chapter of this thesis.

TABLE IV.VII
MODEL TEMPERATURE RESULTS

Motor Location	Temperature [°C]
Rotor DE	170.8
Rotor NDE	259.8
Stator Slot DE	194.2
Stator Slot NDE	242.5
Bottom End Winding NDE	230.2
Bearing DE	93.5
Bearing NDE	88.0

Chapter 5: Reduced-Order thermal Model (ROM).

In this chapter the Reduced Order Model (ROM) is introduced and applied for the same model object of this thesis. In the first subsection, the method is presented together with all the advantages and downsides. Then the application of the ROM based on the machine learning is illustrated for the prediction of the case study motor temperature in transient, in order to reduce the time of the simulation from the order of magnitudes of days to seconds.

Chapter 5.1: Introduction to ROM.

A Reduced Order Model (ROM) is a high-fidelity dynamic model simplification that retains the main behavior and significant effects, with the aim to reduce solution time and storage capacity requested for highly complex models.

Typical duty cycle of traction motors or, more in general, of motors employed in E-mobility are characterized by thousands of operating points. Full-model simulations can be very time consuming especially for 3D model where both thermal and fluid dynamics performances want to be explored.

In this case ANSYS Dynamic ROM is employed. This method is based on *Machine Learning* approach to reduce the order of the model for any sort of simulation data. In fact, it can be used for thermal, mechanical electromagnetic or other type of physics without any distinction.

The use of the ROM can be justified with several advantages.

The first benefit is absolutely the decrease of the simulation time with multiplicative factor of 10-100. This is ideal for particular kind of study like parametric analysis with the aim to improve the design and the motor performances. In addition, it is also very useful for the implementation of Digital Twins and near real-time applications.

Another upside is the reducing of the model size. This brings numerous advantages especially for the reduction of the memory capacity necessary for the storage of the model compared to the mesh-based solvers.

In the other hand, one downside is surely represented by the need to have training data. This data can be calculated from a model previously run in a 3D solver what requires earlier worktime and calculations. This does not suit very well demands in different contexts like design phase or the need to have quick and fast results without creating previous data.

A typical work-process that leads to the set up of a complete reduced-order model is shown in Fig.4.19. As described, at the beginning a source 3D model is employed with the aim to extrapolate 3D simulation data. Subsequently, from these learning data the extraction of a ROM is performed and

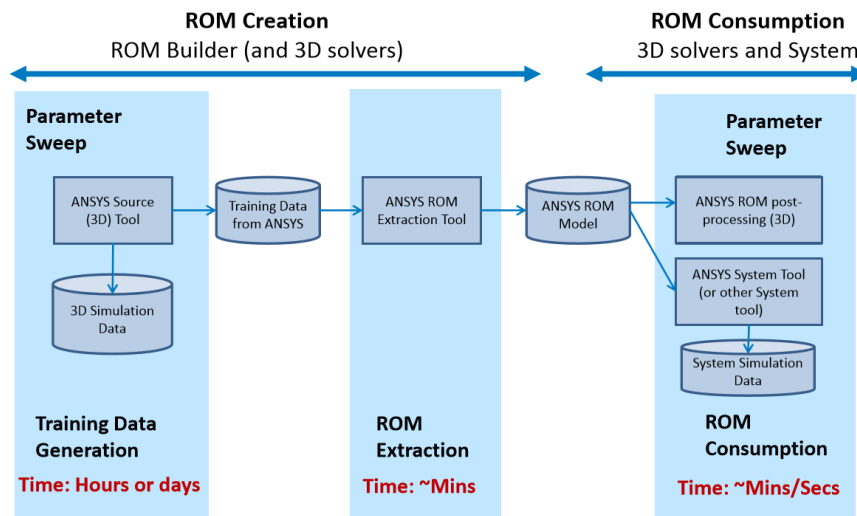


Figure 5.1 Typical ROM Workflow.

model in the reduced form is built. Once the ROM creation phase is complete, the ROM consumption can start and can be used efficiently.

Chapter 5.2: Dynamic ROM technology.

The technology behind the machine learning is based on a non intrusive-method; it is a general algorithm and it does not fit just a specific physics but it can be applied to any kind of problem and model. The physics of the problem object of the simulation can be either non linear or linear. Once

the learning data are provided, the objective of the method is to build a reduced-order model of a generic dynamic system as:

$$\dot{X}(t) = f(X(t); B(t))$$

$$X(0) = X_0$$

Where:

- X is the vector of the solutions. The size of this vector is n (each component is a model output) and this vector is time dependent.
- B is the vector that contains all the excitations of the model. This vector has size n_{exc} and it is also a function of the time.
- f is a non-linear function of both B and X .
- X_0 is the vector that contains all the initial conditions: all the variables are evaluated at the first timestep.

The model is realized thanks to learning data. These pre-calculated data are formed of one or more history variations of the vector X and the relative excitations B . The data are created by more numerical computations from the earlier CHT model. After the ROM is built, the dynamic reduced-order model can be used to compute the history variations of X corresponding to each history variation of B .

In addition to the creation of the dynamic ROM, also a static ROM is created and it is used to conduct several parametric studies on Fluent in steady-state. After the parametric ROMs are produced, they are used to evaluate 3D model of the case study motor to rapidly explore the variation of results as illustrated in Fig. 4.20.

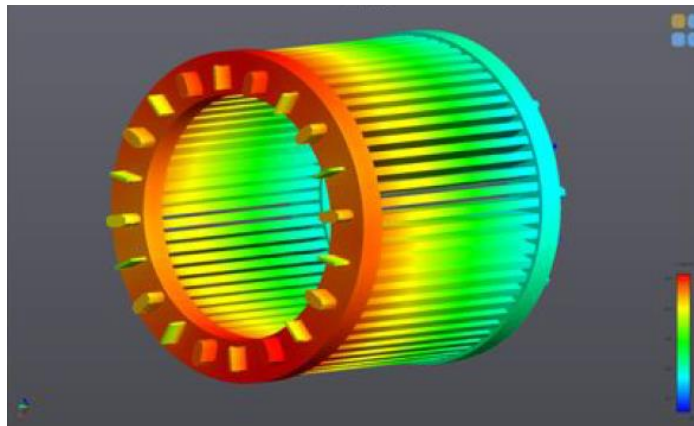


Figure 5.2 Static ROM 3D visualization of the motor.

Chapter 5.3: ROM transient results.

In order to create the ROM and to test its validity for the under-case study motor, a realistic duty cycle typical of traction applications for E-mobility provided from ABB is used. The total cycle studied is a 1500 s cycle and it is used for both creating the learning data and test the ROM.

The first 500 s are employed to implement the learning phase, while the remaining 1000 s are used for the validation process.

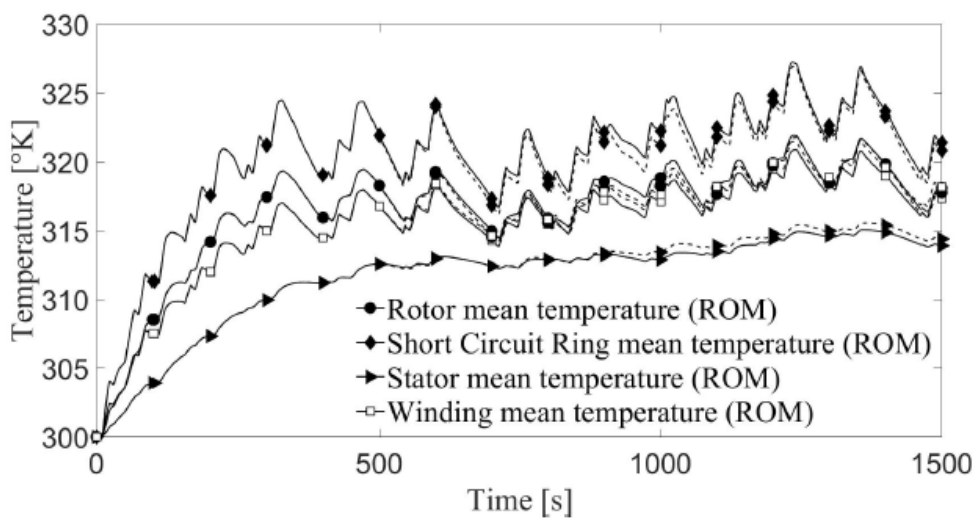


Figure 5.3 Reduced-Order Model results

In the picture Fig. 5.3 is illustrated the comparison between the results achieved with the ROM and mesh-based full model. It is evident that a good agreement between the two methods is reached and this is showing the high accuracy of the dynamic ROM.

In fact from the data can be noted that the maximum absolute error is less than 1 Kelvin in all the parts of the motor and the maximum deviation is in the winding where the position of the conductors, but also of the PT sensors is pretty aleatory.

One of the most achievement of this machine learning based method is the computation time: the time employed to the ROM to run the whole transient cycle is less than 1 second compared to the days of the full model.

Chapter 6: Experimental Setup: model validation.

In this last chapter, the experimental setup for the airflow and temperature measurements are presented. Once the model is implemented properly, airflow and temperature laboratory test are carried out with the aim to validate the numerical calculations. First, the air velocity is measured to compare the results with the CFD behavior of the model in ANSYS. In addition, the steady-state temperatures are then compared with the ones obtained in Fluent.

Chapter 6.1: Case Study Motor.

As abovementioned, laboratory setups are carried out with the scope to make a comparison between the numerical results generated from the CHT tridimensional model realized in ANSYS and the airflow and temperature measurements made in the ABB laboratories.

The case study motor is an ABB motor, built and designed by the company and it is chosen for this study based on its complexity. Open self-ventilated traction motor are known to be very challenging from the thermo-fluid dynamic point of view since they are characterized by a pretty complex cooling system.

The motor cooling system include axial inlets applied to the cover plate, radial outlets, ducts inside both the rotor and stator lamination. This allows the creation of three different parallel path for the airflow not connected between each other represented by the stator ducts, rotor ducts and airgap.

The air is sucked by a radial fan through the radial inlets and ducts, and it is expelled towards the radial inlet in order to cool the motor down. In addition, small blades are also present on the short-circuit rotor bars to provide extra-turbulence in the ends parts of the motor.

TABLE VI.I
CASE STUDY MOTOR

Data	Value
V_{nom}	1100 V
I_{nom}	170 A
P_{nom}	245 kW
ω_{rot}	1914 rpm

In Tab. VI.I the rating data of the motor are listed and in Fig 6.1 the motor is shown.

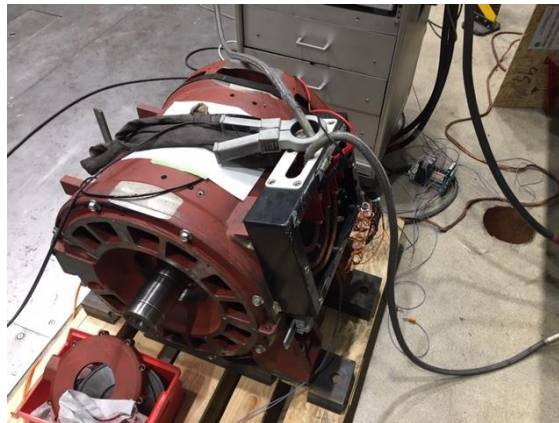


Figure 6.1 Case study motor in ABB laboratory.

Chapter 6.2: Airflow measurements.

Once the model is implemented in ANSYS and the CFD computation is run, it is of vital importance to carry out experimental measurements in order to validate the tridimensional model. In

fact, during the model implementation, several simplifications are adopted in order to reduce the complexity of the model and consequently the computation time.

The setup is realized in the ABB laboratories in the Traction Motors business unit in Västerås, Sweden. The laboratory setting is illustrated in Fig.6.2 and it is built in accordance with the rules relating to the flow measurements.

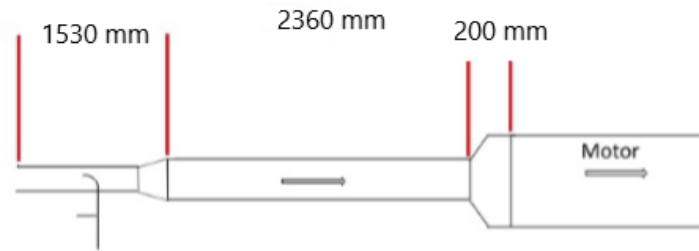


Figure 6.2 Scheme of the airflow measurement setup.

Three different channels are used, each of them with a different diameter. This is essential since the flow entering the inlets has to be laminar and devoid of any kind of turbulence.

The real setup is shown in Fig. 6.3 and Fig. 6.4 where is illustrated the long pipes used in the ABB laboratory with a diameter of 1530 mm, 2360 mm and 200 mm respectively, and the connection with the case study motor.

The measurements of the velocity of the air are conducted at the same speed (rotor and fan speed) of the simulations as shown in Table VI.II where are indicated the speed of the motor for each simulation and measure, and the comparison between experimental and simulation results in terms of mass flow rate [kg/s].



Figure 6.3 Air flow measurement setup and connection to the motor.



Figure 6.4 Airflow measurement setup.

TABLE VI.II MODEL AND MEASUREMENTS RESULTS

	ANSYS Model	Experimental results	Corrected Results
Speed [rpm]	Mass Flow Rate [kg/s]	Mass Flow Rate [kg/s]	Mass Flow Rate [kg/s]
750	0.15575	0.13622	0.1479625
1500	0.30903	0.288966257	0.2935785
2250	0.46685	0.437444395	0.4435075
3000	0.62566	0.584913833	0.594377
3750	0.77856	0.724019231	0.739632
4110	0.85978	0.785482838	0.816791

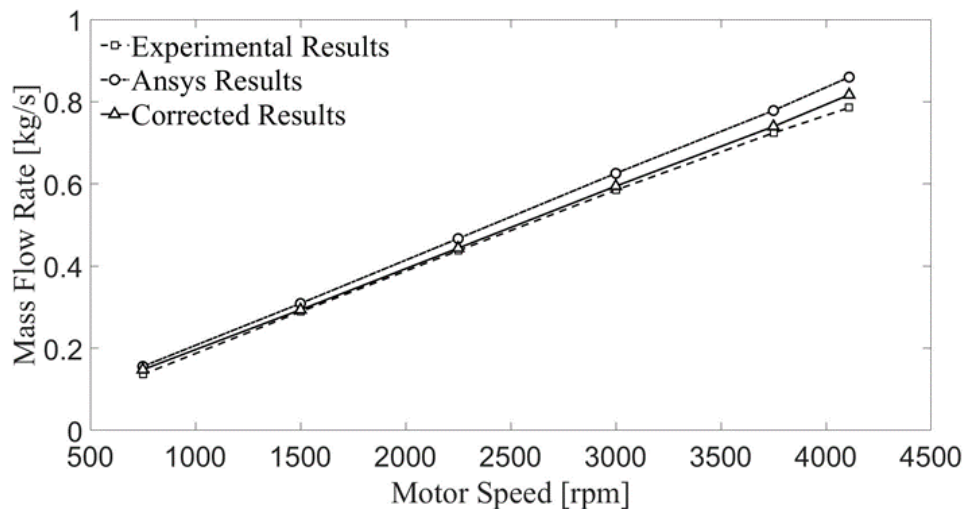


Figure 6.5 Comparison between experimental and simulation results considering the filter grill factor.

As illustrated in the table, there is a third column where the *Corrected Results* are reported. These values take into account a simplification of the model based on the fact that the filter grill is not implemented in the 3D CAD. From the ABB engineers' experience, this grill is used to affect the pressure drop of about 5%. For this reason a filter factor of 0.95 is applied to the ANSYS results.

The comparison is better highlighted in the chart in Fig. 6.3. In this graphic, it is shown that a very good agreement is achieved between the experimental and simulation results within the error range of 5%. If the filter factor grill is applied for the mentioned reasons, the error range is even lower.

Chapter 6.3: Temperature measurements in steady-state conditions.

Once the Conjugate Heat Transfer model is completed, it is possible to run very quickly thermal simulation in steady-state conditions. In contrast with transient simulations, the steady-state ones are not time consuming due to the efficient method used in this thesis and the simplification applied to the model where only the parts significant from the thermal point of view are considered. Thanks to these reasons, the simulation time of the complete model for both thermal and fluid-dynamic calculations is reduced in the order of 7 minutes.

The results of the model are then compared to the laboratory ones in order to validate the CHT model. For this aim an experimental setup for the measure of the temperature in the different parts of the motor is arranged in the ABB laboratory. The scope of this test is to apply the rated voltage and current to the machine for all the time needed to bring the motor in steady-state thermal condition.

The test conditions are illustrated in Tab. VI.III and they are maintained for about two hours. It is necessary to underline that for all the test the values of voltage and current are not kept equal to the rated ones, but the real values are surely lower within a range of 10-20%.

In order to measure accurately the temperature behavior in the different components of the motor, PT1000 sensors are employed.

In Fig. 6.4 the temperature evolution during the test is evaluated for a time duration of 250 min.

TABLE VI.III
THERMAL SETUP CONDITIONS

Data	Value
V_{nom}	1100 V
I_{nom}	160 A
P_{nom}	230 kW
ω_{rot}	2163 rpm

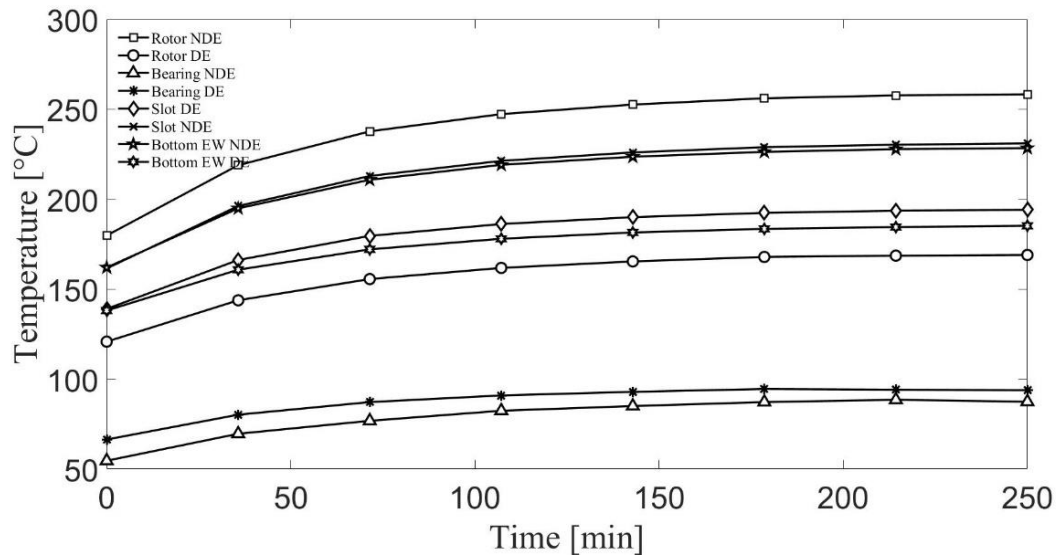


Figure 6.6 Temperature evolution measured at motor different parts by the PT1000 sensors.

The aim of this chapter is however to use these experimental results to validate the model made in Ansys. Since the machine is considered almost in steady-state condition at the end of the test, the final temperature values of the test are compared with the one calculated in Fluent.

As shown in Tab. VI.IV a very good agreement is reached between the simulation and experimental results

TABLE VI.IV
COMPARISON BETWEEN EXPERIMENTAL AND
SIMULATION RESULTS

Location	Experimental Results [°C]	Model Results [°C]
Rotor DE	169.0	170.9
Rotor NDE	258.3	259.9
Slot DE	194.1	194.2
Slot NDE	231.0	242.5
Bottom EW NDE	228.4	230.3
Bearing DE	93.8	93.5
Bearing NDE	87.4	88.0

Chapter 7: Conclusions and Future work.

In this paragraph, a final summary about the results achieved from this thesis study is presented. In addition, ideas and purposes for future works are discussed as consequences of the results reached and studies carried out.

Chapter 7.1: Final Summary.

In this thesis an efficient thermal model to study the thermal behavior of traction motors has been completed.

The model has been implemented following several steps in order to provide a reference literature for the topic object of the study.

In the first part, only the radial fan is modeled, and this shows how a starting modeling of the cooling fan can be useful and increment the accuracy of the final model. In this way the proper functioning of the propeller model is assured and then inserted in the whole motor model.

As second step, the entire cooling system is designed and implemented in ANSYS in order to run CFD simulation incorporating the fan, ducts and airgap. A very good agreement is achieved with the experimental results obtained from the setup conducted in the ABB laboratories, with an error within the 5% range. To adjust the results and to make them closer to the reality, a filter grill factor is applied to the ANSY results to take into account the pressure drops and the decrease of airflow velocity. This showed an even better match with the experimental values.

For the thermal design of the machine, several considerations and approaches have been explained and presented. First, the model has been simplified with the aim to consider only the parts of the motor and the aspects relevant from the thermal point of view. Then, the model is implemented including the previous cooling system tested with the CFD simulations and a Conjugate Heat Transfer model has been built. This takes the big advantage of not calculating apart and importing the convective heat transfer coefficients since they are calculated simultaneously in Fluent. More studies have been conducted in order to model properly the stator slots and end windings. These represent for sure the most complicate parts for the electrical motor thermal design and huge upsides from this study have been noticed. Regarding the stator slot implementation, the Short Transient Test for the evaluation of an equivalent thermal capacitance and resistance of the whole stator slot has proved to be extremely useful and accurate in predicting the thermal behavior of the machine. In fact, a very good agreement between the temperature measurement done with the PT100 sensors and the temperature obtained from the simulations is reached, proving the validity of the CHT model in ANSYS.

Regarding the transient computation, since the computational cost in ANSYS Fluent can be very high, a Reduced Order Model (ROM) is employed and duty cycle characteristic of electric motors for E-mobility usages has been run. Also in this case, the ROM proved its high accuracy and a heavy reduction of the simulation time from days to seconds.

Chapter 7.1: Future Works.

The thermal design of electrical motors is becoming increasingly important, acquiring equal importance with respect to electromagnetic design. In this study, an open self-ventilated traction motor is considered, but it would be of great interest to apply and to test the presented method for other kinds of motors and other types of cooling systems.

One of the aspects that is worth deepening is surely represented by the estimation of the losses in the different active parts and lamination of the motors. This could be realized with combined electromagnetic and thermal simulation by using multiphysics approaches.

It is also important to underline that one of the most difficult aspects in predicting the thermal behavior of electrical machines is represented by the bad implementation of the stator slots and the inexact estimation of the many contact thermal resistance inside them. This can certainly be a theme of study deserving interest.

Scientific Publications.

This thesis project has resulted in the production of the following publications in Congresses and Journal.

Publications in Congresses:

1st Publication L. Boscaglia, F. Bonsanto, S. Nategh, A. Boglietti, C. Scema, "Conjugate Heat Transfer Model for Self Ventilated Traction Motors", IEEE Energy Conversion Congress and Expo (ECCE), Baltimore (MD), Sept. 2019.

2nd Publication A. Boglietti, S. Nategh, E. Carpaneto, L. Boscaglia, C. Scema, "An Optimization Method for Cooling System Design of Traction Motors", IEEE International Electric Machines and Drives Conference (IEMDC), San Diego (CA), May 2019.

3rd Publication C. Scema, S. Nategh, A. Boglietti, L. Boscaglia, D. Ericsson, "A Hybrid Thermal Modeling Method for Traction Motors Used in Duty-Cycles", IEEE International Electric Machines and Drives Conference (IEMDC), San Diego (CA), May 2019.

Publications in Journal:

L. Boscaglia, S. Nategh, F. Bonsanto, A. Boglietti, C. Scema "Numerically-based Reduced-order Thermal Modeling of Traction Motors" IEEE Industry Applications Society (IAS) -SUBMITTED.

Bibliography

- [1] S. Nategh, D. Lindberg, O. Aglen, R. Brammer and A. Boglietti, Review and Trends in Traction Motor Design: Electromagnetic and Cooling System Layouts, 2018 XIII International Conference on Electrical Machines (ICEM), Alexandroupoli, 2018, pp. 2600-2606.
- [2] S. Nategh, H. Zhang, O. Wallmark, A. Boglietti, T. Nassen and M. Bazant, Transient Thermal Modeling and Analysis of Railway Traction Motors, in IEEE Transactions on Industrial Electronics, vol. 66, no. 1, pp. 79-89, Jan. 2019.
- [3] S. Nategh, Thermal Analysis and Management of High-Performance Electrical Machines, Ph.D. Dissertation, KTH Royal Institute of Technology, Stockholm, Sweden, June 2013.
- [4] C. Scema, S. Nategh, A. Boglietti, L. Boscaglia, D. Ericsson, A Hybrid Thermal Modeling Method for Traction Motors Used in Duty-Cycles, IEEE International Electrical Machines and Drives Conference (IEMDC), San Diego, CA, USA, May 2019.
- [5] S. Nategh, A. Boglietti, E. Carpaneto, C. Scema, L. Boscaglia, An optimization method for cooling system design of traction motors, International Electric Machines and Drives Conference (IEMDC), May 2019.
- [6] D. A. Staton and A. Cavagnino, Convection Heat Transfer and Flow Calculations Suitable for Analytical Modelling of Electric Machines, IECON 2006 - 32nd Annual Conference on IEEE Industrial Electronics, Paris, 2006, pp. 4841-4846.
- [7] D. A. Howey, P. R. N. Childs and A. S. Holmes, Air-Gap Convection in Rotating Electrical Machines, in IEEE Transactions on Industrial Electronics, vol. 59, no. 3, pp. 1367-1375, March 2012.
- [8] A. Boglietti, M. Cossale, S. Vaschetto and T. Dutra, Winding Thermal Model for ShortTime Transient: Experimental Validation in Operative Conditions, in IEEE Transactions on Industry Applications, vol. 54, no. 2, pp. 1312-1319, March-April 2018.
- [9] A. Boglietti, R. Bojoi, S. Rubino and M. Cossale, Load Capability of Multiphase Machines under Normal and Open-Phase Fault Conditions, 2018 IEEE Energy Conversion Congress and Exposition (ECCE), Portland, OR, 2018, pp. 242-247.
- [10] P. Pescetto, S. Ferrari, G. Pellegrino, E. Carpaneto and A. Boglietti, Short-Time Transient Thermal Model Identification of Multiple Three-Phase Machines, 2018 IEEE Energy Conversion Congress and Exposition (ECCE), Portland, OR, 2018, pp. 222-228.

- [11] D. Staton, A. Boglietti and A. Cavagnino, Solving the more difficult aspects of electric motor thermal analysis in small and medium size industrial induction motors, in IEEE Transactions on Energy Conversion, vol. 20, no. 3, pp. 620-628, Sept. 2005.
- [12] A. Boglietti, E. Carpaneto, M. Cossale and S. Vaschetto, Stator-Winding Thermal Models for Short-Time Thermal Transients: Definition and Validation, in IEEE Transactions on Industrial Electronics, vol. 63, no. 5, pp. 2713-2721, May 2016.
- [13] S. Nategh, S. Øvrebø, S. Mahdavi and O. Wallmark, Thermal modeling of a permanent magnet machine built using Litz wire, 2015 International Conference on Electrical Systems for Aircraft, Railway, Ship Propulsion and Road Vehicles (ESARS), Aachen, 2015, pp. 1-6.
- [14] D. Staton, A. Boglietti and A. Cavagnino, Solving the more difficult aspects of electric motor thermal analysis, IEEE International Electric Machines and Drives Conference, 2003. IEMDC'03., Madison, WI, USA, 2003, pp. 747-755 vol.2.
- [15] ANSYS Learning Hub <https://www.ansys.com/services/learning-hub>
- [16] Advanced Transient Thermal Modeling of Traction Motors in COMSOL, Claudio Scema, Politecnico di Torino, Aprile 2019.

Acknowledgments.

I am so grateful to be able to thank a large amount of people who contributed to make this travel more pleasant and unique.

I really appreciated to work with professor Boglietti for this master thesis project. I have got impressed by his professionalism and I thank him for everything he taught me during these months.

One of the people I will never thank enough is Shafigh Nategh. I want to thank him first for his friendship, and then for the professional and engineer that made me become. I couldn't imagine a better mentor than him.

Undoubtedly, there is my big family composed by my sisters, my brother, the new “-in law-members” and especially my lovely mum, without whom I would not be anyone and everything would be harder and sadder. Thank you very much for always being there.

Thank to my dear friends. My roommate Fabio with whom I will never quarrel enough, my friend Carmen with whom to stop laughing is really really hard, my dearest Diletta who is always present and with whom I have "luck" in common, and then there is Giulia who never stops to surprise me with its oddities.

Thank you, thank you from the bottom of my heart.

I also want to thank Claudio, the friend with whom I shared this project and the stay in Sweden and then there is Alessandro, my second brother without whom I can't really imagine my life.